Distribution Category:
Magnetic Fusion Energy
(UC-20)

ANL/FPP/TM--207

DE86 015007

ANL/FPP/TM-207

ARGONNE NATIONAL LABORATORY
9700 South Cass Avenue
Argonne, Illinois 60439

LIQUID-METAL FLOW IN A RECTANGULAR DUCT WITH A NON-UNIFORM MAGNETIC FIELD

by

John S. Walker

Department of Theoretical and Applied Mechanics
University of Illinois at Urbana-Champaign
Urbana, Illinois 61801

April 1986

Study Supported by
Office of Fusion Energy
U. S. Department of Energy

TABLE OF CONTENTS

LIST OF FIGURES

LIST OF FIGURES (Continued)

LIQUID-METAL FLOW IN A RECTANGULAR DUCT WITH A NON-UNIFORM MAGNETIC FIELD

By
John S. Walker

ABSTRACT

This paper treats liquid-metal flow in rectangular ducts with thin conducting walls. A transverse magnetic field changes from a uniform strength upstream to a weaker uniform strength downstream. The Hartmann number and the interaction parameter are assumed to be large, while the magnetic Reynolds number is assumed to be small. If the magnetic field changes gradually over a long duct length, the velocity and pressure are nearly uniform in each cross section and the flow differs slightly from locally fully developed flow. If the magnetic field changes more abruptly over a shorter duct length, the velocity and pressure are much larger near the walls parallel to the magnetic field than in the central part of duct. Solutions for the pressure drops due to the magnetic field change are presented.

1. INTRODUCTION

In a self-cooled liquid-metal blanket for a magnetic-confinement fusion reactor, liquid lithium or a litnium-lead mixture circulates through the reactor to collect the energy and to breed the tritium to fuel the plasma. For a toroidal reactor geometry (tokamak), the principal magnetic field is in the toroidal direction, and the field strength in tesla is given by 36/r, where r is distance in meters from the reactor's axis [1]. In the region occupied by the blanket, the magnetic field strength varies from 3 to 8 tesla. Recent advances in plasma physics indicate that stable plasma confinement may be possible with slightly weaker magnetic fields, but the variation in toroidal field strength is intrinsic in the tokamak geometry. The walls of the ducts carrying the liquid metal must be metal because both hot liquid lithium and high neutron fluxes degrade the strength of most electrical insulators. The pressure drop in a magnetohydrodynamic (MHD) duct flow is proportional to the thickness of the duct's walls, so the walls are made as thin as possible. A thorough understanding of three-dimensional liquid metal flows in ducts with thin conducting walls and with strong non-uniform magnetic fields is needed for blanket design calculations.

Holroyd and Walker [2] present analytical solutions for a straight circular pipe with a thin conducting wall and with a transverse magnetic field which varies from one uniform strength upstream to a different uniform strength downstream. The non-uniform magnetic field region is confined to a pipe length L_m which is comparable to the inside radius of the pipe L, and both uniform field strengths are assumed to be large. Walker [3] presents an extension of this analysis to the case with the magnetic field strength decaying to zero downstream instead of approaching a large uniform value.

For a rectangular duct with thin conducting walls and with a transverse magnetic field whose strength varies along the duct, there are boundary layers adjacent to the walls which are parallel to the magnetic field (side layers). These side layers carry a significant fraction of the total flow as high-velocity sheet jets adjacent to the sides, and they are an important part of the electric current circuit. Walker [4] treats these side layers for the three-dimensional flows in expansions and contractions with uniform transverse magnetic fields. Walker [5] presents the boundary value problems governing

the side layers in a rectangular duct with a transverse magnetic field whose strength varies over a duct length L_m which is comparable to L, where L is half the distance between the sides for a rectangular duct. These boundary value problems are formidable and no solutions are presented. Here, we assume that $L_m >> L$, and this assumption makes the boundary value problems tractable. In a tokamak, the magnetic field strength varies from 3 to 8 tesla over a duct length of 7.5 m if the duct's centerline is perpendicular to the tokamak's axis, while the distance between the duct walls parallel to the magnetic field is 0.4 m or less ($L \leq 0.2$ m) [1]. Therefore, this assumption is appropriate for fusion reactor blankets. The present results indicate that this analysis is appropriate for $L_m > 6L$. If we apply the present analysis to a case with $L_m < 6L$, then the essential physics is correct, but an axial derivative which would actually smooth transitions is erroneously neglected. However, the present analysis also reveals an implicit assumption behind the boundary value problems presented by Walker [5] for $L_m = O(L)$, which is not valid for real thin conducting ducts. In particular, the solutions of the boundary value problems presented by Walker [5] would grossly overestimate the pressure drop due to three-dimensional effects Δp_{3D}, while the present analysis would almost certainly be closer and would be conservative with a slight overestimation.

If the value of L_m/L is extremely large, the axial field gradient has negligible effect and the solution at each cross section is given by the solution for fully developed flow with the local value of the magnetic field strength. The locally fully developed flow solution serves as a reference solution and deviations from it indicate the magnitude of the three-dimensional effects. It turns out that the locally fully developed flow is realized for $L_m/L >> c^{-1/2}$, where $c = \sigma_w t/\sigma L$ is the small wall conductance ratio and t is the thickness of the walls, while σ_w and σ are the electrical conductivities of the walls and liquid metal. For a typical case, the axial velocity deviates from that for locally fully developed flow by 6.9% and 1.2% for $L_m = 2Lc^{-1/2}$ and $L_m = 5Lc^{-1/2}$, respectively. For a typical fusion blanket, $c = 0.01$. As the value of L_m/L is reduced from these extremely large values, the fraction of the total flow, which is carried by high-velocity sheet jets adjacent to the sides, increases, and the velocity in the inviscid core region becomes non-uniform with a larger velocity near the sides

than at the plane of symmetry midway between the sides. As L_m/L decreases further, while still being large, the velocity in the core becomes zero and all the flow is carried by the side layers. For $1 \ll L_m/L \ll c^{-1/2}$, there are two boundary layers adjacent to each side. As the flow and electric current in the core become more concentrated near the sides, the core evolves into an inviscid outer side layer adjacent to each side. This outer layer is separated from the side by the same viscous side layer which is now the inner side layer. The inner side layer carries even more of the total flow than it did when part of the flow was distributed over the entire cross section. If we continue reducing L_m/L until this ratio is O(1) and we bring back the axial derivatives neglected here, then we have the boundary value problems presented by Walker [5]. In this case, the core is essentially stagnant, each outer side layer has an $O(c^{1/2})$ thickness and represents a sheet of axial electric current and each inner side layer carries half of the total flow. If we consider the present analysis for $1 \ll L_m/L = O(c^{-1/2})$ and apply it for the case $L_m = 0.1\ Lc^{-1/2}$, we find that the core solution clearly exhibits flow and electric current concentration near the sides. For a typical case, $u_c < 0.025$ for $|z| < 0.5$, but u_c increases rapidly as $|z|$ increases beyond 0.5 and reaches $u_c = 3.5$ at $z = \pm 1$. Here u_c is the axial core velocity normalized by U_o which is the average axial velocity, and z is the coordinate perpendicular to the sides normalized by L. Similarly, almost all the transverse pressure variation is confined to $0.5 < |z| < 1$, where the pressure serves as a stream-function for the axial electric current density. However, each inviscid outer side layer which is beginning to emerge from the core solution still occupies a quarter of the duct's cross section, so they are certainly not thin enough to be considered boundary layers for $L_m = 0.1\ Lc^{-1/2}$. If $c = 0.01$, this case corresponds to $L_m = L$, which should be the case for the boundary value problems presented by Walker [5]. While the flow is tending toward this case, it has certainly not reached it.

Walker [5] seeks an asymptotic solution as $c \to 0$ with $L_m/L = O(1)$. This analysis implicitly assumes that $c^{1/2}L_m/L \to 0$. In practical situations, $c^{1/2}L_m/L$ is probably never less than 0.1 and the flow for this value is still far from that for $c^{1/2}L_m/L \to 0$. The analysis of Walker [5] predicts that the axial electric current in the non-uniform field region is confined to the thin outer side layers and the electrical resistance of these layers is large

because of their thinness. The large resistance restricts the electrical current circualtion which gives a small Δp_{3D}. In reality, the axial electric current in each direction is spread over a quarter of the cross section even for $L_m = L$, so the actual electrical resistance is smaller than that of the thin outer side layers, the total current circulation is larger and Δp_{3D} is larger. Therefore, the solution of the boundary value problems presented by Walker [5] would underestimate the extra pressure drop due to three-dimensional effects.

In the present analysis, there is (1) an upstream fully developed flow in the upstream uniform magnetic field, (2) an upstream transition region in which the effects of the axial magnetic field gradient are significant but the field strength deviates from its upstream uniform value by only a small, namely $O(c^{1/2})$ amount, (3) a gradually varying magnetic field region in which the magnetic field strength is changing but axial derivatives are small, (4) a downstream transition region, and (5) a downstream fully developed flow. The analysis indicates that each transition region extends a distance of 3L into the gradually varying field region. If $L_m > 6L$, the flow manages to reach the gradually varying field solution in some central region, the two transition regions do not interact, and the present analysis is valid. For $L_m < 6L$, the gradually varying field region is gone and the two transition regions are merged into one region in which the magnetic field is changing by an O(1) amount. The flow entering the merged transition region begins to evolve toward the gradually varying field solution, but never reaches it. Instead, the evolution reverses back toward fully developed flow. Therefore, the axial derivative, which is neglected here, prevents the flow from reaching the severity of the flow concentration near the sides which would occur if the gradually varying field solution were reached. If we use the present predictions for Δp_{3D} for $L_m < 6L$, we have the pressure drop for a full transition from fully developed flow to the gradually varying field solution and back to fully developed flow. The real flow only makes part of this transition and only requires part of this pressure drop. Therefore, the present predictions are valid for $L_m > 6L$ and are conservatively approximate for $L_m < 6L$. This assumes that the strength of the weaker magnetic field is roughly half of that of the stronger magnetic field. If the weaker field is only one-tenth the stronger field, the critical value of L_m/L is somewhat

greater than 6, while if the weaker field is nine-tenths of the stronger field, it is less than 6.

2. GOVERNING EQUATIONS AND BOUNDARY CONDITIONS

The ratio of the induced magnetic field, which is produced by the electric currents in the liquid metal and in the duct walls, to the applied magnetic field, which is produced by an external magnet, is given by $c^{1/2}R_m$. Here $R_m = \mu\sigma U_0 L$ is the magnetic Reynolds number and μ is the magnetic permeability for the liquid metal and duct walls. Both c and R_m are small for a fusion blanket, so we neglect the induced magnetic field. The applied magnetic field is governed by

$$\underset{\sim}{B} = -\underset{\sim}{\nabla}\psi, \qquad \nabla^2\psi = 0 \tag{1}$$

where ψ is the magnetic potential function. The faces of the present magnet are shown in Figure 1 and are located at

$$y = \begin{cases} \pm\beta^{-1} d, & \text{for } x \leq 0 \\ \pm\beta^{-1} d\,[1 + \varepsilon(\beta - 1)x], & \text{for } 0 \leq x \leq \varepsilon^{-1} \\ \pm d, & \text{for } x \geq \varepsilon^{-1} \end{cases}$$

where the coordinates are normalized by L, $\varepsilon = L_m/L$ and $\beta > 1$, so that the pole faces are closer together upstream than downstream. The characteristic magnetic field strength, B_0, is chosen as the weaker uniform magnetic field strength downstream. The magnet is assumed to be very wide in the z direction, so that $\underset{\sim}{B} = B_x(x,y)\,\hat{\underset{\sim}{x}} + B_y(x,y)\,\hat{\underset{\sim}{y}}$, where $\hat{\underset{\sim}{x}}$ and $\hat{\underset{\sim}{y}}$ are unit vectors. The magnet poles are assumed to have a very large magnetic susceptibility, so that $\underset{\sim}{B}$ inside the poles is decoupled from the outside, and $\psi = \pm d$ at the lower and upper pole faces, respectively. In Sections 3 and 4, we take $\varepsilon = \gamma c^{1/2}$, i.e., $L_m = L\,\gamma^{-1}c^{-1/2}$, where γ is an O(1) parameter, i.e., γ remains finite and non-zero as $c \to 0$. In the central or gradually varying field region, we compress the axial coordinate by substituting $x = Xc^{-1/2}$. In this region the solution of the equations (1) gives

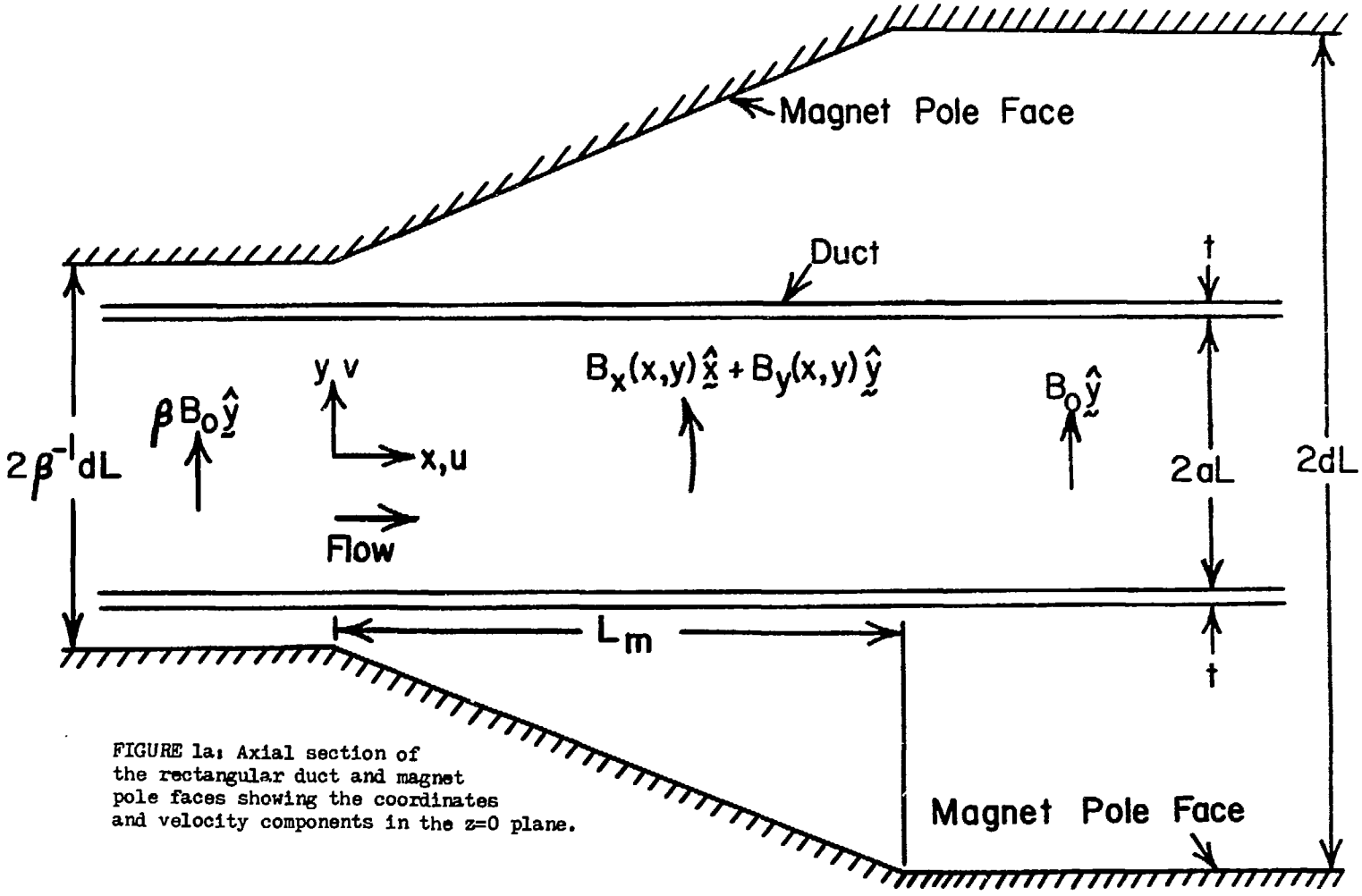

FIGURE 1a: Axial section of the rectangular duct and magnet pole faces showing the coordinates and velocity components in the z=0 plane.

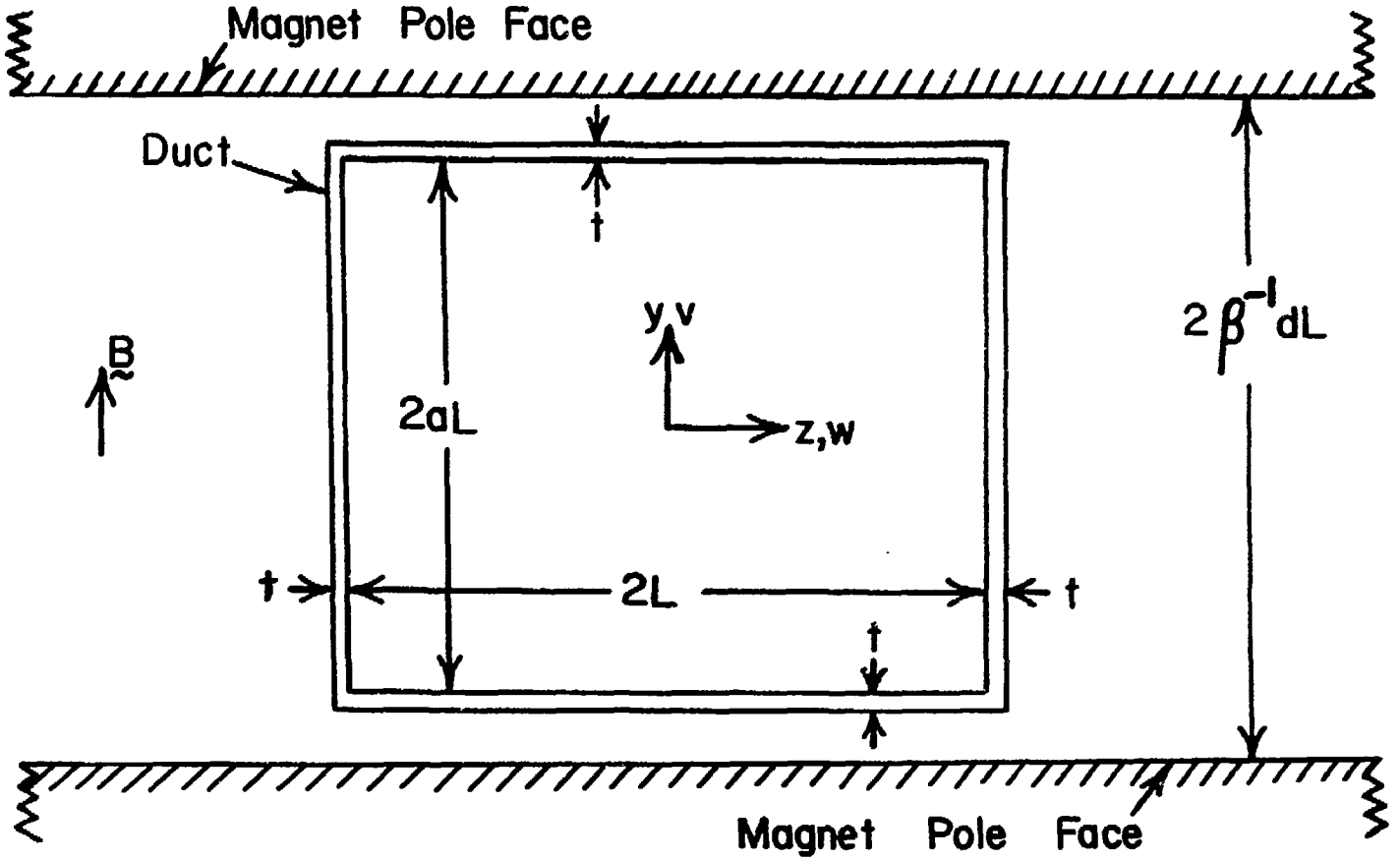

FIGURE 1b: Cross section of the rectangular duct and magnet pole faces showing the coordinates and velocity components in the x=0 plane.

$$B_y = \beta[1 + (\beta - 1)\,\gamma X]^{-1} + O(c) \tag{2a}$$

$$B_x = -\gamma c^{1/2}\,\beta(\beta - 1)\,y\,[1 + (\beta - 1)\,\gamma X]^{-2} + O(c^{3/2}) \tag{2b}$$

for $0 < X < \gamma^{-1}$. In the upstream transition region near $x = 0$, the magnetic field must match the upstream uniform field $\beta\hat{y}$ as $x \to -\infty$ and the gradually varying field (2) as $x \to \infty$. The solution of the equations (1) near $x = 0$ is

$$B_y = \beta - \gamma c^{1/2}\,\frac{\partial \psi_u}{\partial y}(x,y) + O(c) \tag{3a}$$

$$B_x = -\gamma c^{1/2}\,\frac{\partial \psi_u}{\partial x}(x,y) + O(c) \tag{3b}$$

where

$$\psi_u = \begin{cases} -\beta^{-1}(\beta - 1)\,\Psi(x,y;\beta), & \text{for } x < 0 \\ \beta(\beta - 1)xy - \beta^{-1}(\beta - 1)\,\Psi(-x,y;\beta), & \text{for } x > 0 \end{cases} \tag{3c}$$

$$\Psi(x,y;\beta) = d^2\pi^{-2} \sum_{n=1}^{\infty} (-1)^n\, n^{-2} \sin(\beta n\pi y/d)\, \exp(\beta n\pi x/d) \tag{3d}$$

In the downstream transition region near $x^* = x - \varepsilon^{-1} = 0$, the magnetic field must match the gradually varying field (2) as $x^* \to -\infty$ and the downstream uniform field $\hat{y}$ as $x^* \to \infty$. The solution is

$$B_y = 1 - \gamma c^{1/2}\,\frac{\partial \psi_d}{\partial y}(x^*,y) + O(c) \tag{4a}$$

$$B_x = -\gamma c^{1/2}\,\frac{\partial \psi_d}{\partial x^*}(x^*,y) + O(c) \tag{4b}$$

where

$$\psi_d = \begin{cases} \beta^{-1}(\beta - 1)\,x^*y + \beta^{-1}(\beta - 1)\,\Psi(x^*,y;1), & \text{for } x^* < 0 \\ \beta^{-1}(\beta - 1)\,\Psi(-x^*,y;1), & \text{for } x^* > 0 \end{cases} \tag{4c}$$

In section 5, we treat the case $c^{1/2} << \varepsilon << 1$, so that ε and c are independent small parameters. Then we compress the axial coordinate with $x = X\varepsilon^{-1}$. For this case, the magnetic field in the gradually varying field and transition regions is given by the same expressions (2-4) with γ and $c^{1/2}$ replaced by 1 and ε, respectively.

The ratio of the electromagnetic body force to the inertial "force" is characterized by the interaction parameter $N = \sigma B_0^2 L/\rho U_0$, where ρ is the liquid metal's density. For a typical self-cooled blanket $N = 10^4$, so that inertial effects are small. We neglect inertial effects everywhere and then use the inertialess solutions to define the required condition on N. In the core regions, $N >> 1$ is sufficient to insure that inertial effects are negligible. However, in the side layers, the axial velocity is large and in the transition regions near $x = 0$ and ε^{-1}, this large axial velocity changes over an O(1) duct length as some of the flow migrates from the core to the side layers or back. To neglect inertial effects in these subregions requires that $N >> M^{3/2}$, where $M = B_0 L (\sigma/\rho\nu)^{1/2}$ is the Hartmann number and ν is the liquid metal's kinematic viscosity. Since $M = 10^4$ for a typical blanket, this condition is not met. However, there are several reasons to believe that the present inertialess analysis provides good predictions even though $N = O(M)$ instead of $N >> M^{3/2}$. For the fully developed flows at $x = \pm\infty$ the inertialess solutions with the high-velocity sheet jets near $z = \pm 1$ are valid for any N since there are no axial variations. In the downstream transition region for a typical case, the fraction of the total flow carried by each side layer Q_s must decrease from 0.073 to 0.068 in a duct length equal to 6L. The condition $N >> M^{3/2}$ assumes that the side layer velocity is $M^{1/2}U_0$ in a duct length equal to L. The results for this typical case indicate that the maximum side layer velocity is roughly $0.25\ M^{1/2}U_0$ and changes by only $0.017\ M^{1/2}U_0$ in a duct length equal to 6L. Therefore, the relative error in the inertialess solution for the downstream transition region side layer can be expected to be $0.00071M^{3/2}N^{-1}$, which is only 7.1% for $N = M = 10^4$. There is a slightly larger change in Q_s in the side layer for the upstream transition region, but here the magnetic field strength is βB_0, so that the local interaction parameter and Hartmann number are given by $\beta^2 N$ and βM respectively. The $\beta^{-1/2}$ in the local inertialess error more than cancels the effect of the larger velocity change. In the side layers, in the gradually varying field region

for the same typical case, Q_s decreases from 0.098 to 0.073 over a duct length equal to $L_m = L\varepsilon^{-1}$, so the relative error in the inertialess solution is smaller here by a factor of ε. The typical case discussed here has $\gamma = 1$, $\beta = 2$, and $\alpha = cM^{1/2} = 1$. If we consider a much larger slope for the diverging magnet pole faces by increasing γ and β, then inertial effects would become more important, particularly near $x = 0$ and ε^{-1}. In the extreme case with $L_m = L$, the boundary value problems presented by Walker [5] indicate that Q_s must decrease from 0.5 to 0.068 for the side layers near $x = \varepsilon^{-1}$. However, the present analysis for $L_m = 0.1\, Lc^{-1/2}$ shows that Q_s only changes from 0.22 to 0.068 here and this is the same case if $c = 0.01$. The present results give a relative inertialess error of $0.023M^{3/2}N^{-1}$, which is unfortunately 233% for $N = M = 10^4$, so inertial effects are not negligible for such abrupt magnetic field changes. The inertial effects would prevent the full acceleration of the side layers in the gradually varying field region, but the interaction of the transition regions for $L_m = L$ does the same thing, so Q_s never reaches 0.22. In addition, inertial effects would disturb the downstream fully developed flow to larger values of x^*. As the product $\gamma(\beta - 1)$ increases, inertia changes the velocity profiles near $x = 0$ and ε^{-1} before it changes Δp_{3D} for two reasons. Inertia first becomes important in the transition regions, but these regions make no significant contributions to Δp_{3D}. This pressure drop is due entirely to the gradually varying field region in which the inertial effects are smaller by a factor of ε. In addition, the side layer flows involve an acceleration followed by an almost identical deceleration, so that the pressure changes due to inertial effects tend to cancel as long as the flows are stable. The critical values of N for the instabilities of the side layers which generate vortices parallel to the magnetic field are much smaller than 10^4. As with any asymptotic analysis the error in the predictions of the present inertialess analysis as a function of N for a given duct and magnet can best be defined by experiments. previous MHD experiments with reasonably detailed velocity and pressure measurements have been restricted to $N < 50$. At Argonne National Laboratory, experiments for the present situation, with $N = 100 - 1000$ or larger and with detailed measurements are planned for sometime in the next year or two.

The inductionless, inertialess, dimensionless equations governing the liquid metal flow are

$$\nabla p = \underset{\sim}{j} \times \underset{\sim}{B} + M^{-2} \nabla^2 \underset{\sim}{v}, \qquad \nabla \cdot \underset{\sim}{v} = 0 \tag{5a,b}$$

$$\underset{\sim}{j} = -\nabla\phi + \underset{\sim}{v} \times \underset{\sim}{B}, \qquad \nabla \cdot \underset{\sim}{j} = 0 \tag{5c,d}$$

Here p, $\underset{\sim}{j}$, $\underset{\sim}{v}$, and ϕ are the pressure, electric current density, velocity, and electric potential function, normalized by $\sigma U_0 B_0^2 L$, $\sigma U_0 B_0$, U_0 and $U_0 B_0 L$, respectively (See [6], Chapter 2). The dimensionless applied magnetic field $\underset{\sim}{B}$ is given by one of the expressions (2-4) or by $\beta\hat{\underset{\sim}{y}}$ and $\hat{\underset{\sim}{y}}$ far upstream and downstream, respectively. The present duct has a constant rectangular section (see Figure 1). Here, we assume that all four walls have the same thickness, t, because this is the case for the future experiments at Argonne National Laboratory. In a fusion blanket, the walls parallel to the toroidal magnetic field may be thicker than those perpendicular to this field. The extension of the present analysis to ducts with different wall thicknesses is straightforward [7]. If $t \ll L$, then the variation of the electric potential function between the inside and outside surfaces of each wall is negligible. The electric potential in the wall, ϕ_w, is simply given by the value in the liquid metal at the inside surface of the wall. The tangential components of the electric current density in the wall are then given by

$$\underset{\sim}{j}_w = -(\sigma_w/\sigma)\nabla\phi_w \tag{6}$$

Integration of the equation (5d) inside the wall then gives the thin conducting wall boundary condition [4] on the liquid-metal variables evaluated at the inside surface of each wall:

$$j_y = \mp c \left(\frac{\partial^2 \phi}{\partial x^2} + \frac{\partial^2 \phi}{\partial z^2} \right) \qquad \text{at } y = \pm a \tag{7a}$$

$$j_z = \mp c \left(\frac{\partial^2 \phi}{\partial x^2} + \frac{\partial^2 \phi}{\partial y^2} \right) \qquad \text{at } z = \pm 1 \tag{7b}$$

In addition to applying the boundary conditions (7), we must also insure that electric current is conserved at the corners at $y = \pm a$ and $z = \pm 1$. From equation (6)

$$\lim_{y \to \pm a} \frac{\partial \phi}{\partial y}(x,y,-1) = \pm \lim_{z \to -1} \frac{\partial \phi}{\partial z}(x,\pm a,z) \tag{8a}$$

$$\lim_{y \to \pm a} \frac{\partial \phi}{\partial y}(x,y,1) = \mp \lim_{z \to 1} \frac{\partial \phi}{\partial z}(x,\pm a,z) \tag{8b}$$

The velocity must satisfy the boundary and total flow conditions

$$\underset{\sim}{v} = 0 \quad \text{at } y = \pm a, \text{ and at } z = \pm 1 \tag{9a,b}$$

$$\int_{-1}^{1} \int_{-a}^{a} u \, dy \, dz = 4a \tag{10}$$

where the latter is a consequence of choosing the average velocity for U_0. The boundary value problem (5, 7-9) is linear and homogeneous and the solution is scaled by the total flow condition (10). The solution for flow from a region of weaker magnetic field to a region of stronger magnetic field is given by replacing the 4a in the condition (10) with -4a. This simply changes the sign of all solutions given here.

The principal subregions of the flow (see Figure 2) are: (c) the core region in the gradually varying field region for $0 < x < \gamma^{-1}$ if $\varepsilon = \gamma c^{1/2}$ or for $0 < X < 1$ if $c^{1/2} << \varepsilon << 1$ and its side layers (s); (u) the core in the upstream transition region near $x = 0$ and its side layers (us); (d) the core in the downstream transition region near $x = \varepsilon^{-1}$ and its side layers (ds); the upstream (ufd) and the downstream (dfd) fully developed flows which are approached as $x \to \mp \infty$, respectively. Each of these regions is separated from the top and bottom by a Hartmann layer with $O(M^{-1})$ thickness. The Hartmann layer variables satisfy the boundary conditions (9a) and match the adjacent core or side layer variables provided the latter satisfy

$$v = 0, \qquad \text{at } y = \pm a \tag{11}$$

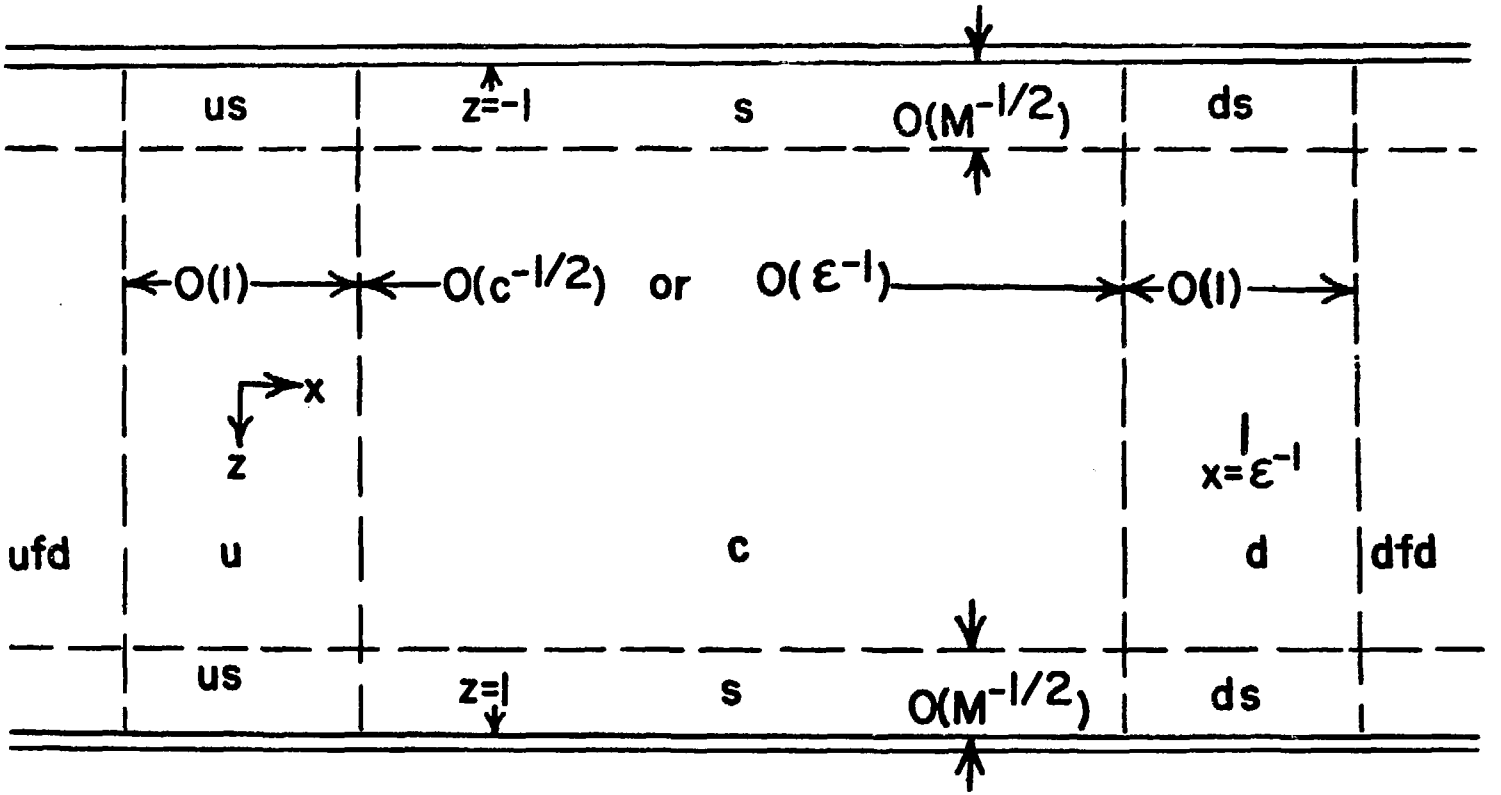

FIGURE 2: Horizontal section in the y=0 plane showing the principal subregions of the flow. All subregions are separated from the top and bottom at y=±a by Hartmann layers.

The jumps in j_y and ϕ across the Hartmann layers are $O(M^{-1})$ and $O(M^{-2})$, respectively, so that the condition (7a) can be applied directly to the core or side layer variables provided $c >> M^{-1}$. The top or bottom and the adjacent Hartmann layer are electrical resistors in parallel. The condition $c >> M^{-1}$ states that the top or bottom has a much smaller resistance than the adjacent Hartmann layer, and that the tangential current in the Hartmann layer is much smaller than that in the top or bottom.

Since typical values are $c = 0.01$ and $M = 10^4$, we assume that $c = \alpha M^{-1/2}$, where α is an $O(1)$ parameter. We are looking for an asymptotic solution for $c \to 0$ and $M \to \infty$ with the restriction that $cM^{1/2} \to \alpha$, a finite, non-zero constant. Each side and adjacent side layer are also electrical resistors in parallel and α is the ratio of the side layer's resistance to the side's resistance. For a given finite α, the tangential electric currents are split between these parallel resistors. The two extreme cases are $M^{-1} << c << M^{-1/2}$ for which all the currents flow in the side layer, and $M^{-1/2} << c << 1$ for which all the currents flow in the side. Walker [4] shows that as $\alpha \to 0$ the solution for $c = \alpha M^{-1/2}$ gives the solution for $M^{-1} << c << M^{-1/2}$ and that as $\alpha \to \infty$ the solution for $c = \alpha M^{-1/2}$ gives the solution for $M^{-1/2} << c << 1$. Therefore, the present analysis includes the two extreme cases as special cases. It also shows precisely how large or small α must be for the simpler extreme case solutions to apply. For a typical three-dimensional flow considered here ($\beta = 2$, $\gamma = 1$, $a = 1$), the solution for $\alpha = 0.1$ still deviates by 5% from the solution for $M^{-1} << c << M^{-1/2}$. For the same case, the solutions for $\alpha = 8$ and 20 deviate by 2.6% and 1.0% from that for $M^{-1/2} << c << 1$.

3. GRADUALLY VARYING FIELD REGION FOR $L_m = L_\gamma^{-1} c^{-1/2}$

In the core the solution for the equations (5) with the appropriate symmetry about $y = 0$ is

$$u_c = B_y^{-1} \frac{\partial \phi_c}{\partial z}, \quad v_c = B_y^{-2}\, y \frac{\partial^2 p_c}{\partial z^2} - \beta^{-1}(\beta - 1)\, \gamma y \frac{\partial \phi_c}{\partial z} \qquad (12a,b)$$

$$w_c = -B_y^{-1} \frac{\partial \phi_c}{\partial X} - B_y^{-2} \frac{\partial p_c}{\partial z}, \quad J_{xc} = B_y^{-1} \frac{\partial p_c}{\partial z} \tag{12c,d}$$

$$j_{yc} = -\beta^{-1}(\beta - 1)\, \gamma y \frac{\partial p_c}{\partial z}, \qquad j_{zc} = -B_y^{-1} \frac{\partial p_c}{\partial X} \tag{12e,f}$$

Here the subscript c denotes the leading terms in the asymptotic expansions for the core variables in the gradually varying field region for $0 < X < \gamma^{-1}$; u_c and ϕ_c are O(1); v_c, w_c, j_{xc} and p_c are $O(c^{1/2})$; j_{yc} and j_{zc} are O(c); $B_y(X)$ is given by the expression (2a) neglecting the O(c) terms; $\phi_c(X,z)$ and $p_c(X,z)$ are unknown integration functions. The boundary conditions (7a, 11) give a pair of equations governing p_c and ϕ_c and these equations only involve derivatives with respect to z. The solutions with the appropriate symmetry about $z = 0$ are

$$p_c = P_c + AB_y a^{-1/2} [\cosh(fz) - \cosh(f)] \tag{13a}$$

$$\phi_c = A \sinh(fz), \quad f(X) = (\beta - 1)\gamma a^{1/2}[1 + (\beta - 1)\gamma X]^{-1} \tag{13b,c}$$

Here A(X) and $P_c(X)$ are unknown integration functions to be determined by the side layer solution, while $P_c = p_c$ at $z = \pm 1$.

Since the flow is symmetric about $z = 0$, we need only treat the side layers at $z = -1$. With the stretched side layer coordinate $\zeta = M^{1/2}(z + 1)$, the equations (5) give

$$w_s = -B_y^{-1} \frac{\partial \phi_s}{\partial X} - \gamma\beta^{-1} (\beta - 1)y \frac{\partial \phi_s}{\partial y} - B_y^{-2} \frac{\partial p_s}{\partial \zeta} \tag{14a}$$

$$u_s = B_y^{-1} \frac{\partial \phi_s}{\partial \zeta}, \quad j_{xs} = B_y^{-1} \frac{\partial p_s}{\partial \zeta} + \gamma\beta^{-1}(\beta - 1)\, B_y y \frac{\partial \phi_s}{\partial y} \tag{14b,c}$$

$$j_{ys} = -\frac{\partial \phi_s}{\partial y}, \qquad j_{zs} = -\alpha B_y^{-1} \frac{dP_c}{dX} + B_y^{-2} \frac{\partial^3 \phi_s}{\partial \zeta^3} \tag{14d,e}$$

$$\frac{\partial v_s}{\partial y} = B_y^{-2} \frac{\partial^2 p_s}{\partial \zeta^2} + \gamma(\beta - 1)\beta^{-1} \quad y \frac{\partial^2 \phi_s}{\partial y \partial \zeta} - \frac{\partial \phi_s}{\partial \zeta} \tag{14f}$$

$$\frac{\partial p_s}{\partial y} = \frac{\partial^2 v_s}{\partial \zeta^2} - \gamma\beta^{-1}(\beta - 1)y \quad \frac{\partial^3 \phi_s}{\partial \zeta^3} - \alpha B_y \frac{dP_c}{dX} \tag{14g}$$

$$B_y^2 \frac{\partial^2 \phi_s}{\partial y^2} = \frac{\partial^4 \phi_s}{\partial \zeta^4} \tag{14h}$$

for $0 < X < \gamma^{-1}$, $-a < y < a$, $0 < \zeta < \infty$. Here u_s is $O(M^{1/2})$, v_s is $O(c^{1/2}M^{1/2})$, ϕ_s and j_{ys} are $O(1)$, w_s and j_{xs} are $O(c^{1/2})$, j_{zs} is $O(M^{-1/2})$ and

$$p = c^{1/2} P_c(X) + c^{1/2} M^{-1/2} p_s(X,y,\zeta)$$

The equations (14f-h) govern the variables v_s, p_s and ϕ_s, while the equations (14a-e) give the other side-layer variables in terms of these three key variables.

Matching the core solution (12, 13) gives the conditions

$$v_s \to 0, \quad \phi_s \to -A \sinh(f) \tag{15a,b}$$

$$p_s \to p_c'(X,-1) - \zeta A B_y a^{-1/2} f \sinh(f), \quad \text{as } \zeta \to \infty \tag{15c}$$

where $p_c'(X,z)$ is the $O(c^{1/2} M^{-1/2})$ perturbation pressure in the core. Walker [4] shows that the $O(1)$ ϕ_w is constant in the sections of the top and bottom adjacent to the side layer and this is compatible with the condition (7a). This result and the condition (11) give the boundary conditions

$$v_x = 0, \quad \phi_x = -A \sinh(f), \quad \text{at } y = \pm a \tag{16a,b}$$

The boundary conditions (7b, 9b) become

$$v_s = 0, \quad \frac{\partial \phi_s}{\partial \zeta} = 0 \tag{17a,b}$$

$$\frac{\partial p_s}{\partial \zeta} = -B_y \frac{\partial \phi_s}{\partial X} - \gamma\beta^{-1}(\beta - 1) B_y^2 y \frac{\partial \phi_s}{\partial y} \tag{17c}$$

$$B_y^2 \frac{\partial^2 \phi_s}{\partial y^2} = \alpha^{-1} \frac{\partial^3 \phi_s}{\partial \zeta^3} - B_y \frac{dP_c}{dX}, \qquad \text{at } \zeta = 0 \tag{17d}$$

The equations (14f,g) and the conditions (15a,c, 16a, 17a,c) constitute a boundary value problem governing v_s and p_s if the solution for ϕ_s is known. This boundary value problem has a solution for any ϕ_s which satisfies a solubility condition. This condition is derived by integrating the equation (14f) from $y = -a$ to $y = a$ and from $\zeta = 0$ to $\zeta = \infty$ and by introducing the conditions (15b,c, 16a, 17c). The resulting condition can be integrated with respect to X to obtain

$$\int_{-a}^{a} \phi_s (X,y,0)\, dy = C\, B_y(X) \tag{18}$$

where C is the constant integration. When we introduce the core and side layer axial velocities (12a, 14b) into the total flow condition (10) and we use the matching between ϕ_c and ϕ_s, we obtain the same condition (18) with $C = -2a$. The solution for ϕ_s gives the $O(M^{1/2})$ axial side-layer velocity u_s which carries part of the total O(1) flow. The fraction of the total flow carried by each side layer Q_s changes along the duct, so that there must be a transfer of O(1) flow between the core and side layers and this requires the $O(c^{1/2})$ transverse velocities w_c and w_s. In the core, u_c is independent of y, but in the side layer u_s has a variation with y which is associated with $\partial\phi_s(X,y,0)/\partial y$. The latter is not zero as long as electric current enters the side at $y = \pm a$ and flows down the side and into the side layer as $j_{zs}(X,y,0)$. Therefore, as the flow is transferred between the core and the side layer, it must be redistributed in the y direction and this requires the $O(c^{1/2}M^{1/2})v_s$. The pressure variation associated with this flow transfer and

vertical redistribution is an $O(c^{1/2}M^{-1/2})$ perturbation p_s of the principal $O(c^{1/2})$ side-layer pressure $P_c(X)$. The solution for the secondary velocities v_s and w_s and the perturbation pressure p_s is guaranteed as long as the primary velocities u_c and u_s satisfy the total flow condition (10) which gives the solubility condition (18) with $C = -2a$. The solutions for v_s and p_s are straightforward, but are not presented here because they provide little additional insight into the flow.

We must also guarantee conservation of electric current at the corners at $y = \pm a$, $z = -1$ with the condition (8a). We modify this condition so that the ϕ on the right-hand side is the core ϕ_c. The modified condition states that the $O(c^{1/2})$ electric current flowing from the side into the corner, plus the $O(c^{1/2})$ current flowing from the side layer into the adjacent part of the top or bottom, must equal the $O(c^{1/2})$ current flowing in the top or bottom adjacent to the core at $z = -1$. This condition is for a duct length with an $O(1)$ ΔX which corresponds to an $O(c^{-1/2})$ ΔX and neglects the axial current in the portion of the top or bottom adjacent to the side layer because this current is $O(c^{3/2}M^{-1/2})$. The condition (8a) becomes

$$\frac{\partial \phi_s}{\partial y}(X,\pm a,0) + \alpha^{-1} \int_0^\infty \frac{\partial \phi_s}{\partial y}(X,\pm a,\zeta)\, d\zeta = \pm \frac{\partial \phi_c}{\partial z}(X,-1) \tag{19}$$

The first and second terms represent the electric currents in the y direction in the side and side layer, respectively. The ratio of these parallel resistors is $\alpha = cM^{1/2}$. If $\alpha \gg 1$, the second term is negligible and all the $O(c^{1/2})$ electric current in the y direction flows through the side. If $\alpha \ll 1$, the first term is negligible, all this current flows through the side layer, ϕ_s decreases to $O(\alpha) = O(cM^{1/2})$ which is small for $M^{-1} \ll c \ll M^{-1/2}$, and the side layers no longer carry any of the $O(1)$ total flow. If (1) we integrate the governing equation (14h) from $y = -a$ to $y = a$ and from $\zeta = 0$ to $\zeta = \infty$, (2) we integrate the thin conducting wall condition (17d) from $y = -a$ to $y = a$, and (3) we introduce the results into the condition (19), it reduces to

$$\frac{dP_c}{dX} = -a^{-1} B_y \frac{\partial \phi_c}{\partial z}(X,-1) = -a^{-1} B_y A\, f \cosh(f) \tag{20}$$

The conservation of electric current condition (8a) has now been extended from the corners at $y = \pm a$, $z = -1$ to the region composed of the side, side layer and adjacent parts of the top and bottom. The condition (20) states that these is no net current across the ΔX length of the plane which is parallel to the side and which separates the core from the side layer. The total $O(c^{1/2})$ electric currents in the z direction in the core and in the adjacent section of the top or bottom, evaluated at $z = -1$, are

$$-2a(\Delta X) B_y^{-1} \frac{dP_c}{dX}, \qquad -(\Delta X) A f \cosh(f)$$

respectively. The electric current flowing from the core into the side layer must return to the top and bottom adjacent to the core in the same cross section. This is true because the axial currents in the side and side layer are both much smaller than $O(c^{1/2})$.

With the expression (20) introduced into the thin conducting wall condition (17d), the solution of the boundary value problem (14h, 15b, 16b, 17b,d) is

$$\phi_s = -A \sinh(f) - A \sum_{n=0}^{\infty} a_n \cos[(2n+1)\pi y/2a] \exp(-\lambda_n \zeta) \times$$

$$[\sin(\lambda_n \zeta) + \cos(\lambda_n \zeta)] \tag{21a}$$

where

$$a_n = 16af \cosh(f)\, \pi^{-3}(-1)^n (2n+1)^{-3} (a + a^{-1}\lambda_n^{-1})^{-1} \tag{21b}$$

$$\lambda_n = \frac{1}{2}[\pi B_y (2n+1) a^{-1}]^{1/2} \tag{21c}$$

The solubility or total flow condition (18) with $C = -2a$ now determines

$$A = B_y[\sinh(f) + 2\pi^{-1} \sum_{n=0}^{\infty} (-1)^n(2n + 1)^{-1}a_n^{-1}] \tag{22}$$

In the next section we show that the $O(c^{1/2})$ pressure at $z = \pm 1$ is constant through the transition regions which match the present solutions at $X = 0$ and γ^{-1} and match the upstream and downstream fully developed flows. We choose $p = 0$ at $x = 0$, $z = \pm 1$, so that p here represents the deviation of the actual pressure from the pressure at these two points. Therefore, the initial condition for the equation (20) is $P_c(0) = 0$. This equation is integrated numerically to get $P_c(X)$. The equations (12, 13, 14b,d,e, 21, 22) now give all core variables and the important side layer variables u_s, j_{ys}, and j_{zs}. The pressure gradient for locally fully developed flow [4] in the gradually varying field region is

$$\frac{dp_{fd}}{dX}(X) = -B_y^2\, a^{-1}[1 + 32a\pi^{-4} \sum_{n=0}^{\infty} (2n + 1)^{-4}(1 + \alpha^{-1}\lambda_n^{-1})^{-1}]^{-1} \tag{23}$$

The actual pressure gradients for both the locally fully developed flow and the three-dimensional flow are $O(c)$, but the axial scale is compressed by $O(c^{1/2})$, so that $p_c(X,z)$ and $p_{fd}(X)$ are both $O(c^{1/2})$. The equation (23) is also integrated numerically from $X = 0$ where $p_{fd} = 0$.

The results for the core and side layers in the gradually varying field region depend on four parameters: a = the aspect ratio of the duct's cross section, α = the ratio of c to $M^{-1/2}$ which reflects the relative electrical resistances of the side and side layer, β = the ratio of the stronger magnetic field strength to the weaker one, and γ = the ratio of $Lc^{-1/2}$ to L_m, so that a large γ means that the magnetic field changes over a short duct length and a small γ means it changes over a long duct length. The gradient of the transverse component of the magnetic field is

$$\frac{dB_y}{dX} = -\beta^{-1}\,(\beta - 1)\,\gamma B_y^2 \tag{24}$$

which varies from $-\beta(\beta - 1)\gamma$ at $X = 0$ to $-\beta^{-1}(\beta - 1)\gamma$ at $X = \gamma^{-1}$, so that the product $(\beta - 1)\gamma$ is an average measure of the magnetic field gradient. The results are relatively insensitive to a unless a is either very large or very small, and only results for a square cross section ($a = 1$) are presented here. The velocity profiles for the side layers are very similar to those presented by Walker [4] with the magnitude of the velocity scaled to reflect the local value of Q_s, so no side layer velocity profiles are presented here. The important side layer result is $Q_s(X)$. Here, we present results for $Q_c(X)$, the fraction of the total flow carried by the core at each cross section, while $Q_s = 0.5(1 - Q_c)$.

Far upstream and downstream $\phi = 1.685z$ and $0.864z$, respectively, for $\alpha = 1$ and $\beta = 2$. At $z = 0$, $\phi = 0$ everywhere, but at $z = 1$, ϕ drops from 1.685 to 0.864, while at $z = -1$, ϕ rises from -1.685 to -0.864. These axial voltage differences drive axial electric currents in the $\pm x$ direction near $z = \pm 1$. For local fully developed flow, the current circulates only in cross sections with current in the +z direction in the core and in the -z direction in the top or bottom. The current circuit is completed by currents in the y direction in the sides and side layers. For the three-dimensional flows treated here, the axial currents due to the axial voltages differences are superimposed on the transverse current for locally fully developed flow. As a result, a current line leaving the side at $z = -1$ in the gradually varying field region first turns in the core and goes far upstream. Many of these current lines cross the $z = 0$ plane in the upstream transition region, while the rest cross it near $X = 0$. The current lines are symmetric about $z = 0$, so they return to the side a $z = 1$ at the same X where they left the side at $z = -1$. Again the electric circuit is completed through the sides, side layers and top and bottom. For all values of γ some of the axial currents complete their circuit in the core of the downstream transition region. Therefore, there are some current lines contained entirely in the liquid metal with current in the $\pm x$ direction near $z = \pm 1$ in the gradually varying field region, current in the +z direction near $X = 0$, and current in the -z direction in the downstream transition region core. For sufficiently large γ, more of the axial current lines are completed in the core rather than in the walls and there is current in the -z direction in the gradually varying field region as well as in the downstream transition core. Wherever the current in

the liquid metal is in the -z direction, it is pumping the flow rather than retarding it, so that the local pressure rises in the flow direction.

Figure 3 presents graphs of p_c and u_c at various cross sections along the gradually varying field region for $\alpha = \gamma = 1$ and $\beta = 2$. The total axial currents in the $\pm x$ direction for $z \gtrless 0$ are always maximum at $X = 0$ where the magnetic field gradient (24) and the axial voltage gradients are maximum. The axial current produces a body force away from the $z = 0$ plane and towards the sides. This body force produces the transverse pressure and velocity variations shown in Figure 3. As X increases, current lines are entering the sides (or completing their circuit at $z = 0$ in the liquid metal for sufficiently large γ), so that the total axial current in either direction decreases, the transverse body force decreases and the transverse variations in p_c and u_c decrease. The transition between the non-uniform velocity $X = 0$ (or 1) and $u = 0.843$ (or 0.864) in the upstream (or downstream) fully developed flow for $\alpha = 1$ and $\beta = 2$ is the role of the upstream (or downstream) transition region at $x = 0$ (or ε^{-1}).

The results for the gradually varying field region depend strongly on γ, as illustrated in Figure 4 for $\alpha = 1$ and $\beta = 2$. Figures 4a-c present u_c and p_c at $X = 0$ since the values here involve the maximum transverse variations for any X. For $\gamma = 0.2$, u_c is very close to u for locally fully developed flow. As γ increases, the flow moves away from the $z = 0$ plane and toward the sides. The core is evolving toward two outer side layers near $z = \pm 1$ which are separated by a nearly stagnant region near $z = 0$. For $\gamma > 6.5$, $u_c(0,0)$ is essentially zero. The overall axial voltage difference is $0.812z$. If the axial current at $X = 0$ is also linear in z, it produces a parabolic pressure variation, $(1 - z^2)$. For $\gamma < 3$, the graphs in Figure 4b have nearly parabolic shapes. For $\gamma > 3$, the axial electric current, like the axial velocity, is becoming concentrated into regions near $z = \pm 1$ with a nearly current-free region near $z = 0$. This results in a steep pressure gradient near $z = \pm 1$ and a more uniform pressure near $z = 0$. At $\gamma = 10$, there is a uniform pressure core for $|z| < 0.6$ and a sheet of axial electric current in each emerging outer side layer for $|z| > 0.6$. As γ increases from zero, the duct length for the axial voltage difference decreases so that the axial voltage gradient increases. As long as the axial current is distributed over the entire cross section ($\gamma < 3$) the magnitude of the total axial current and the pressure

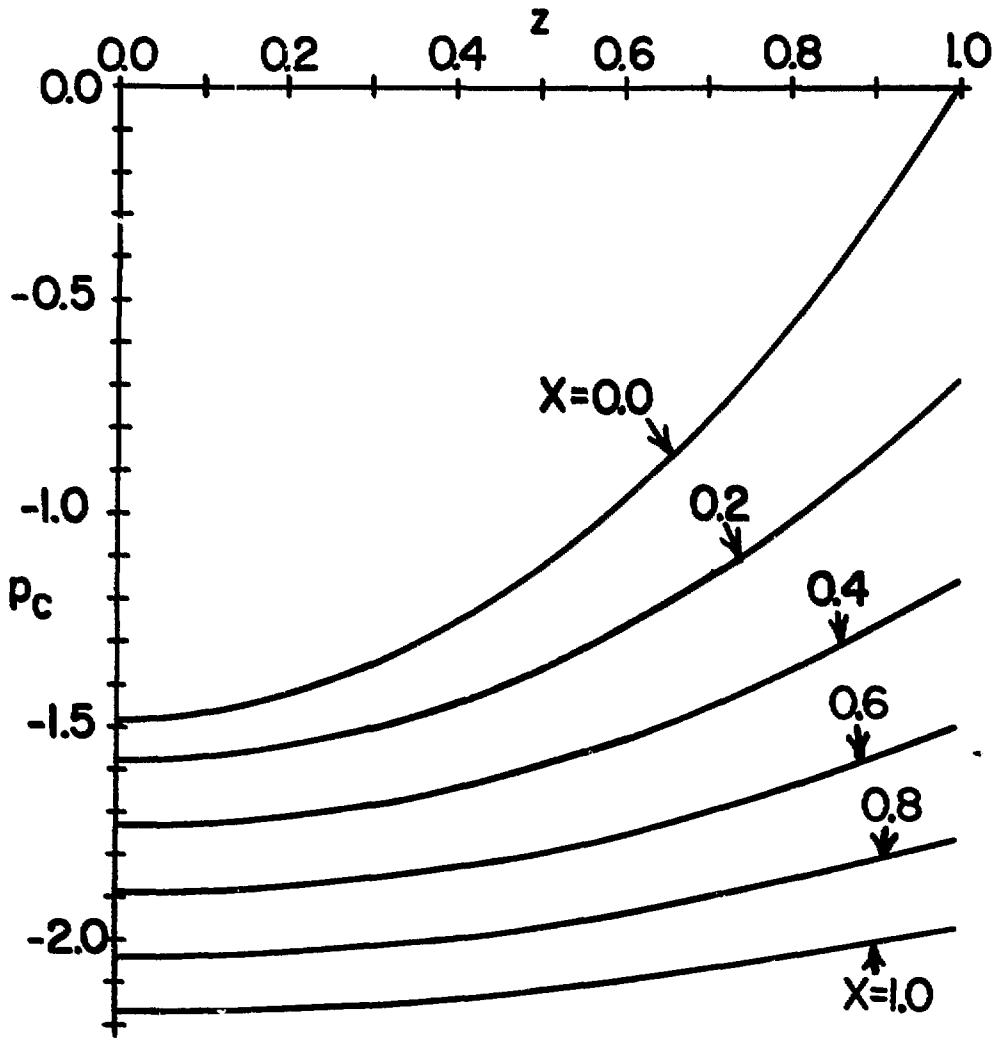

FIGURE 3a: Pressure $p_c(X,z)$ in the core of the gradually varying field region for $\alpha = \gamma = a = 1$ and $\beta = 2$.

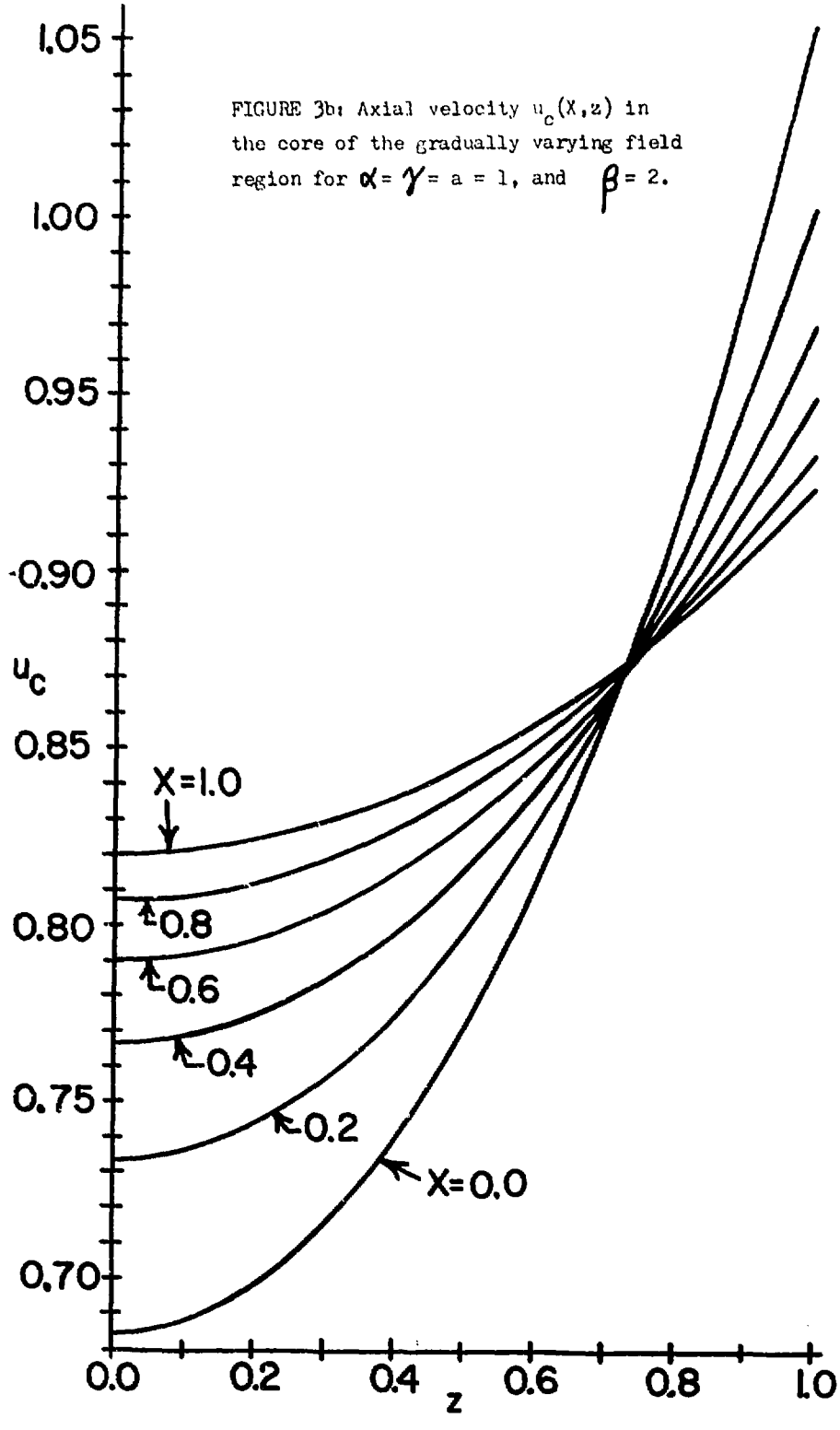

FIGURE 3b: Axial velocity $u_c(X,z)$ in the core of the gradually varying field region for $\alpha = \gamma = a = 1$, and $\beta = 2$.

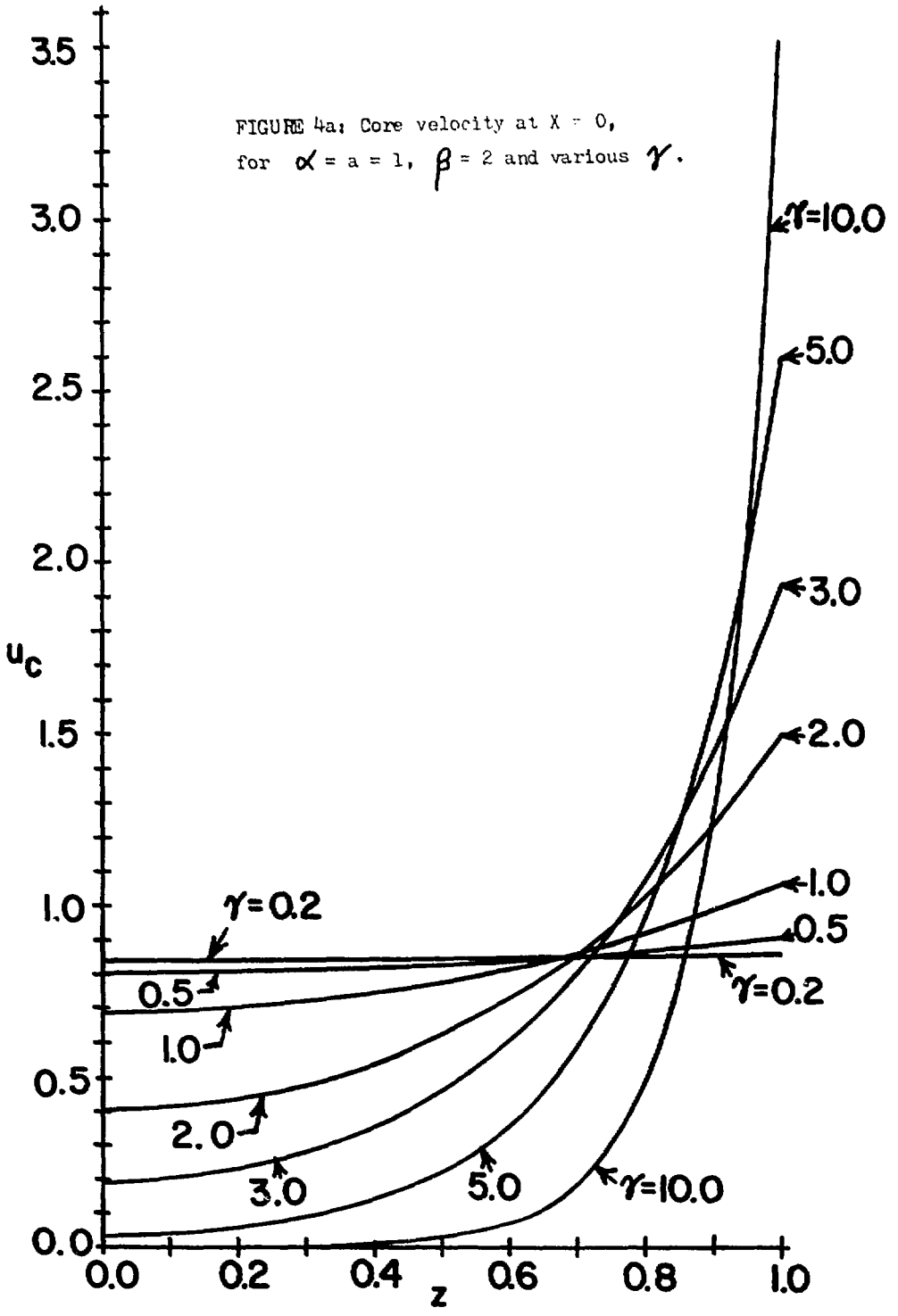

FIGURE 4a: Core velocity at X = 0, for α = a = 1, β = 2 and various γ.

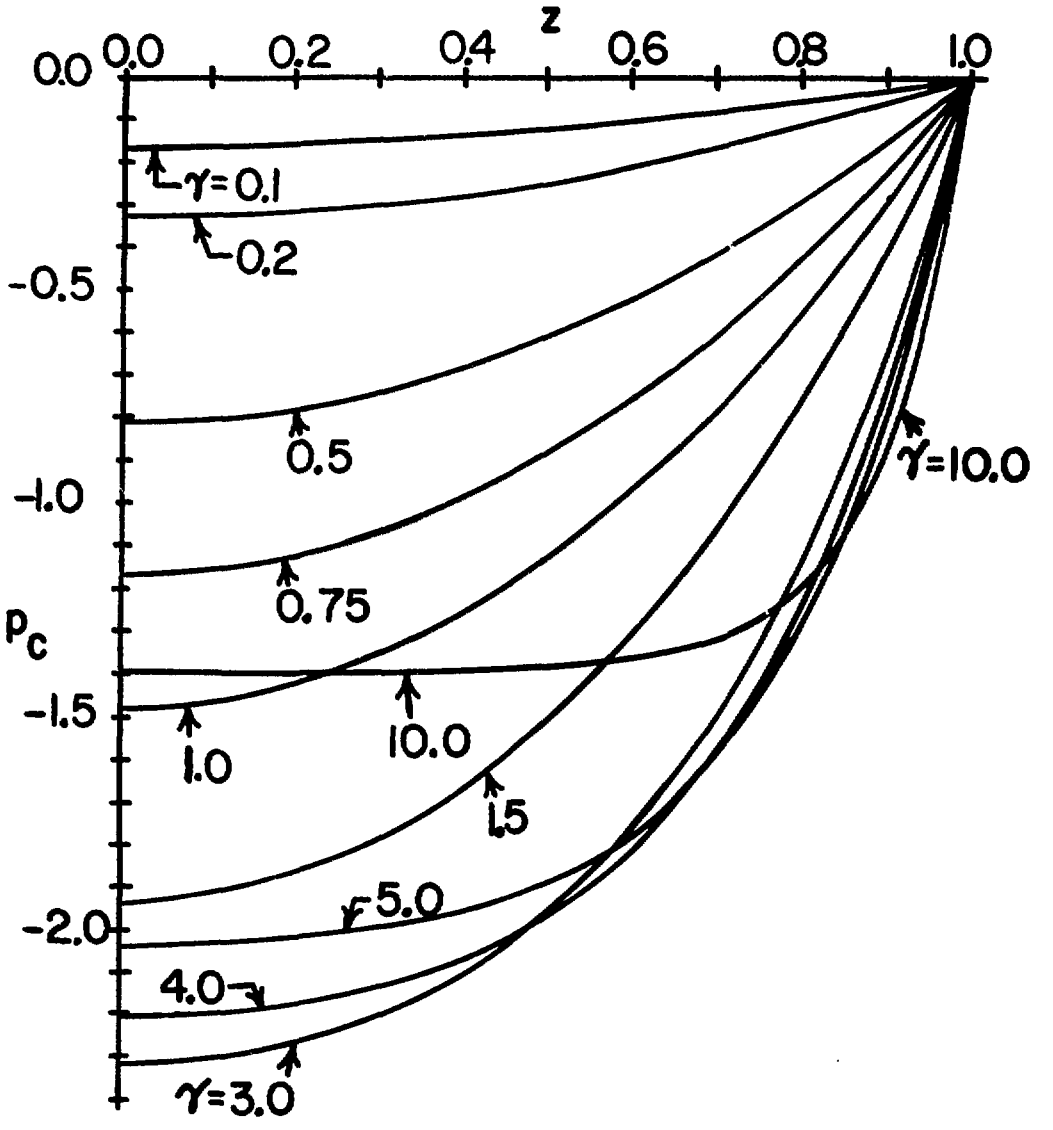

FIGURE 4b: p_c at X=0 for $\alpha = a = 1$, $\beta = 2$ and various γ.

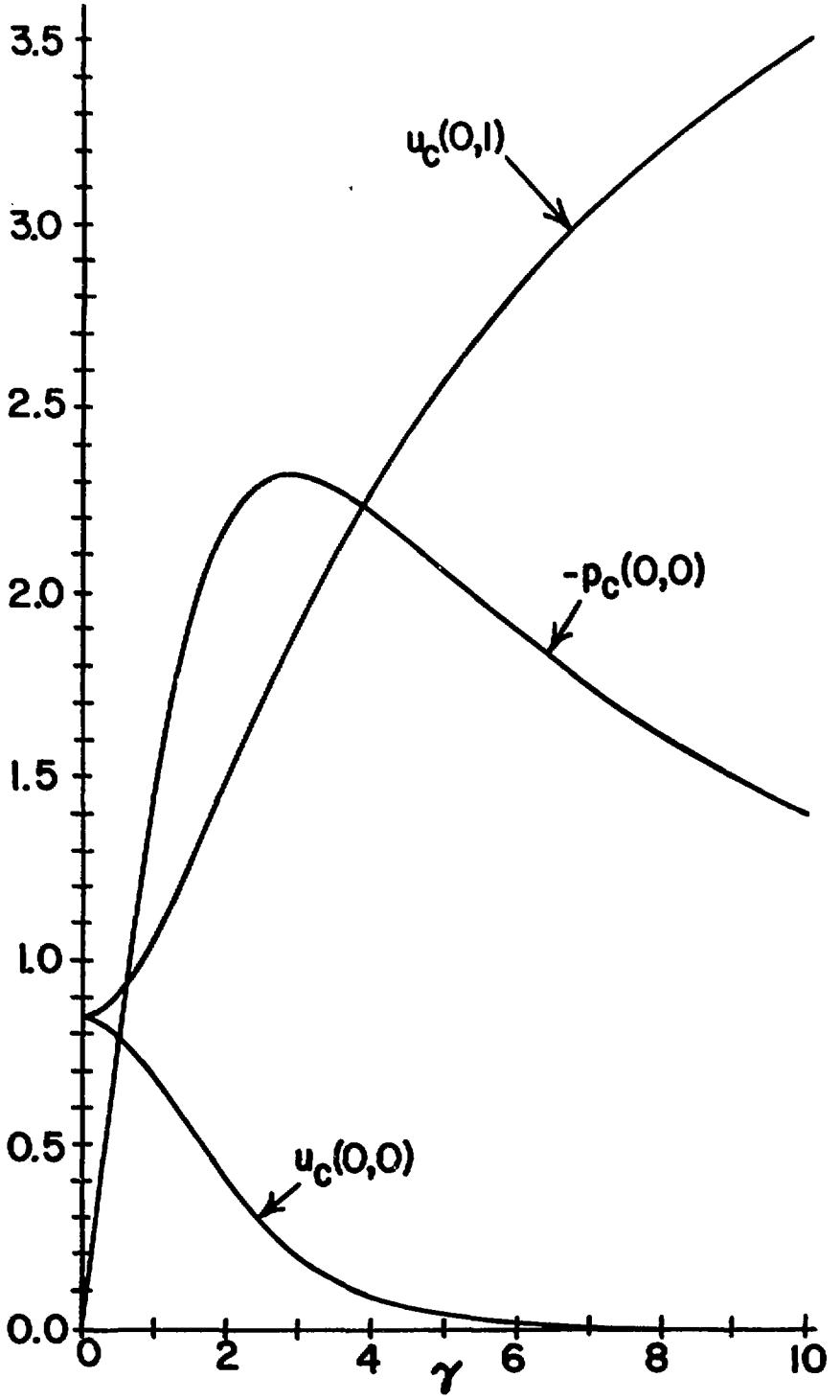

FIGURE 4c: p_c and u_c at z=0 and u_c at z=1, all at X=0, as functions of γ for α = a = 1, and β = 2.

difference between $z = 0$ and $z = \pm 1$ increase as γ increases. However, for $\gamma > 3$, the fraction of the cross section over which j_x is distributed decreases which increases the effective electrical resistnace to axial currents. The increase in the resistance exceeds the increase in the axial voltage gradient as γ increases further, so that the total axial current and the difference between p_c at $z = 0$ and $z = \pm 1$ decrease. Figure 4c illustrates the peak and subsequent decrease of the transverse pressure difference with increasing γ.

Holroyd and Walker [2] show that there are certain characteristic surfaces for liquid metal flows in strong magnetic fields. A characteristic surface is defined by the set of magnetic field lines with the same value of

$$\xi = \int_0^{s_t} [B(s)]^{-1} \, ds$$

where s is the distance measured along the magnetic field line from its intersection with the inside surface of the bottom at $s = 0$ to its intersection with the inside surface of the top at $s = s_t$, while $B(s) = [B_x^2 + B_y^2]^{1/2}$ is the magnetic field strength at each point on the magnetic field line. If ξ is the same for all magnetic field lines (e.g., a uniform magnetic field and parallel top and bottom), then there are no distinct characteristic surfaces and there are relatively few restrictions on $\underset{\sim}{j}$. If ξ varies considerabley, then the electric current in the core must flow along the characteristic surfaces defined by constant values of ξ. In any core region the viscous term in the equation (5a) is negligible and the electromagnetic body force $\underset{\sim}{j} \times \underset{\sim}{B}$ must be balanced by the pressure gradient $\underset{\sim}{\nabla} p$. Therefore $\underset{\sim}{\nabla} \times (\underset{\sim}{j} \times \underset{\sim}{B}) = 0$. This distinguishes a liquid metal from a solid conductor. A solid has a structure which can provide the stress field to balance any body force until yielding occurs. A nearly inviscid, inertialess liquid has only pressure to balance a body force. If a current produced a rotational body force, the fluid would respond violently. The resultant change in $\underset{\sim}{v}$ would change the balance in the Ohm's law (5c), thus changing $\underset{\sim}{j}$ until its body force is irrotational. The characteristic surface derivation involves this irrotationality condition, equation (5d) and the fact

that the normal current to the top and bottom is negligible. The present results help to define the boundary between "free" flows with the same value of ξ for every magnetic field line and "guided" flows with distinct characteristic surfaces for different values of ξ. For the present problem: if $d\xi/dx << c^{1/2}$, then the flow is free; if $d\xi/dx >> c^{1/2}$, then the flow is guided and there is no axial electric current in the core. The present analysis treats the transition case with $d\xi/dx = O(c^{1/2})$, so that the characteristic surface mechanism is pulling the electric current lines but is not strong enough to force perfect alignment with the characteristic surfaces. As γ increases, transverse characteristic surfaces are emerging near $z = 0$ which block the axial electric current here. They do not block the axial current near $z = \pm 1$ because $\partial^2\phi/\partial z^2$ is becoming large near $z = \pm 1$, so that the normal current to the top and bottom from the thin conducting wall condition (7a) is not negligible. The evolution of the core into two outer side layers separated by a region without axial current or velocity corresponds to the emergence of characteristic surfaces which block the axial current and velocity except where transverse voltage gradients in the top and bottom are sufficiently large to drive significant electric currents into or out of the liquid metal at $y = \pm a$. The effective electrical resistance to axial currents increases rapidly with the restriction of these currents to regions near $z = \pm 1$, so that the three-dimensional electrical current circulations are reduced in spite of increasing axial voltage gradients. Therefore, transverse pressure variations and Δp_{3D} peak at certain values of γ and decrease with further increases in γ. Any treatment of three-dimensional effects which ignores the fact that the lack of structure of the liquid metal restricts the three-dimensional current circulation and limits Δp_{3D} grossly overestimates Δp_{3D} (see, for example, Hoffman and Carlson [8]).

Figure 4d presents the axial variation of the pressures at $z = 0$ and at $z = \pm 1$ for three values of γ, as well as $p_{fd}(X)$ for comparison. Here, γp is plotted as a function of γX to give the same axial scales and to make the graph of γp_{fd} the same for all γ. However, the actual axial length for $\gamma = 0.5$ is three time that for $\gamma = 1.5$. For $\gamma = 0.5$, the pressure drop along the sides is only 4% more than that for locally fully developed flow. The pressure at $z = 0$ has a significant drop in the upstream transition region because of the extra current lines crossing the $z = 0$ plane here. Downstream,

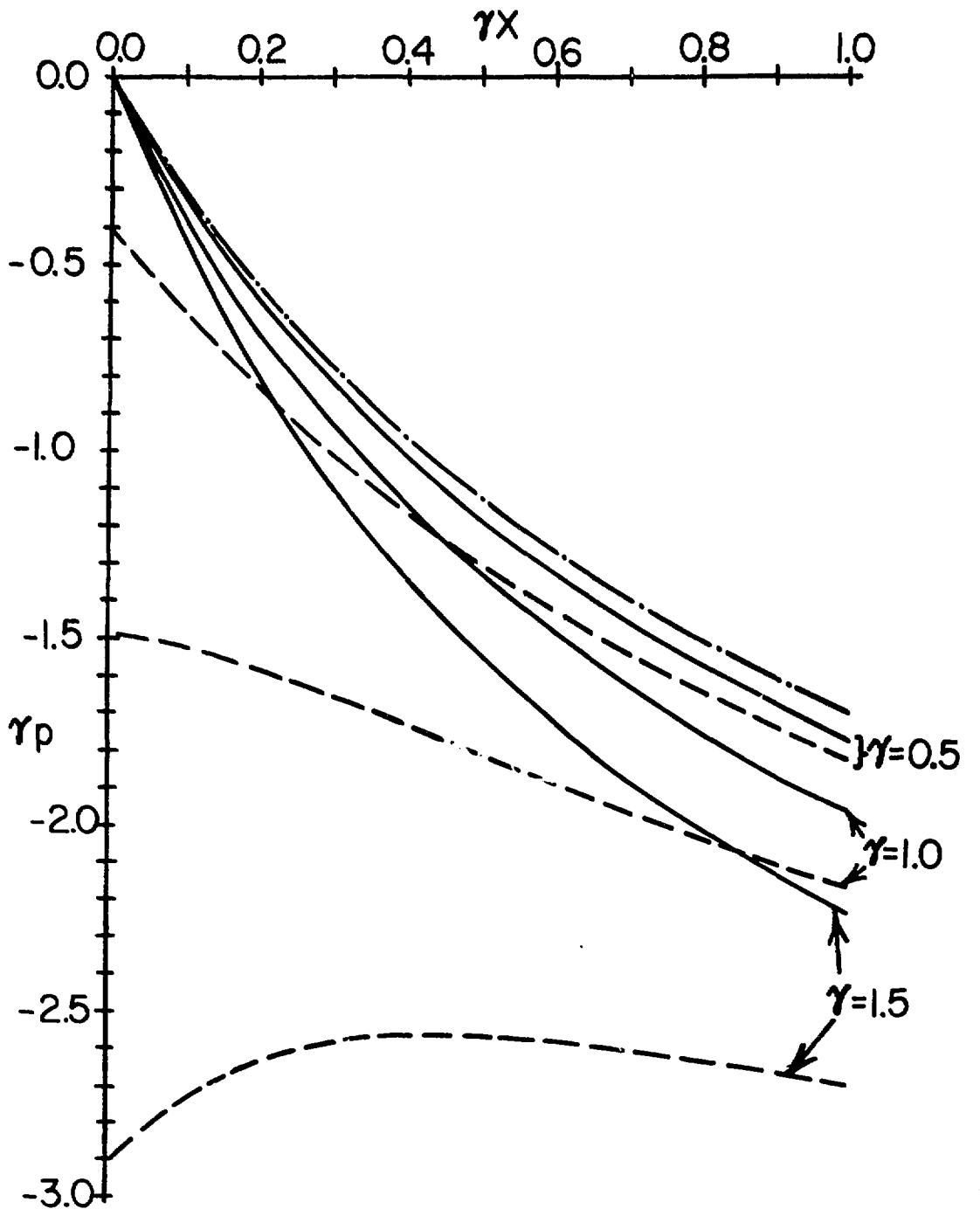

FIGURE 4d: $p_c(X,0)$ (dashed lines), $p_c(X,1)$ (solid lines) and $p_{fd}(X)$ (dot-dash line) for $\alpha = a = 1$, $\beta = 2$ and various γ.

it approaches the pressure at the sides. In the downstream transition region it rises to equal the pressure at the sides because of the current in the -z direction here. For $\gamma = 1$, the pressure drop at $z = \pm 1$ is 15% more than that for locally fully developed flow. The pressure at $z = 0$ has a much larger drop in the upstream transition region, decreases for all X indicating that $j_z > 0$ throughout the gradually varying field region, approaches the pressure at $z = \pm 1$ as X increases, and increases to equal the pressure at $z = \pm 1$ in the downstream transition region. For $\gamma = 1.5$, the pressure drop at $z = \pm 1$ is 32% more than that for locally fully developed flow. The pressure at $z = 0$ drops enormously in the upstream transition region, rises for $0 < X < 0.27$ indicating that $j_z < 0$ at $z = 0$ for these values of X, drops for $0.27 < X < 0.67$, and rises to equal the pressure at $z = \pm 1$ in the downstream transition region. For $\alpha = 1$ and $\beta = 2$: (a) for $\gamma < 1$, p at $z = 0$ drops through both the upstream transition and gradually varying field regions and only rises through the downstream transition region; (b) for $\gamma > 2$, p at $z = 0$ drops enormously through the upstream transition region and then rises through both the gradually varying field and downstream transition regions; (c) for $1 < \gamma < 2$, p at $z = 0$ drops through the upstream transition region, first rises and then drops in the gradually varying field region and finally rises in the downstream transition region.

Figure 4e presents graphs of $Q_c(X)$ for various γ. The graph for $\gamma < 0.2$ is also the graph for locally fully developed flow. If $\alpha >> 1$, all the current in the y direction near $z = \pm 1$ flows through the side which has a much lower electrical resistance than the side layer, and $Q_c = 0.75$ for all fully developed flows at $a = 1$ [4]. If $\alpha << 1$, then all the y current is in the side layer and $Q_c = 1$ for fully developed flows. At $X = 0$, $B_y = \beta$, so that the local Hartmann number is βM. Therefore, the local side layer thickness is $O(\beta^{-1/2} M^{-1/2})$ and the ratio of its resistance to that of the side is $\beta^{1/2} M^{1/2} c = \alpha \beta^{1/2}$. The thinner side layer has more resistance which forces more current into the side and reduces Q_c for local fully developed flow. As X increases, B_y decreases, the side layer thickness increases, more of the current flows in the side layer and Q_c for locally fully developed flow increases. Clearly, Q_s increases dramatically with increasing γ. As γ increases, the flow in the core becomes more concentrated near $z = \pm 1$ and the fraction of the flow carried by high velocity sheet jets in the side layers at

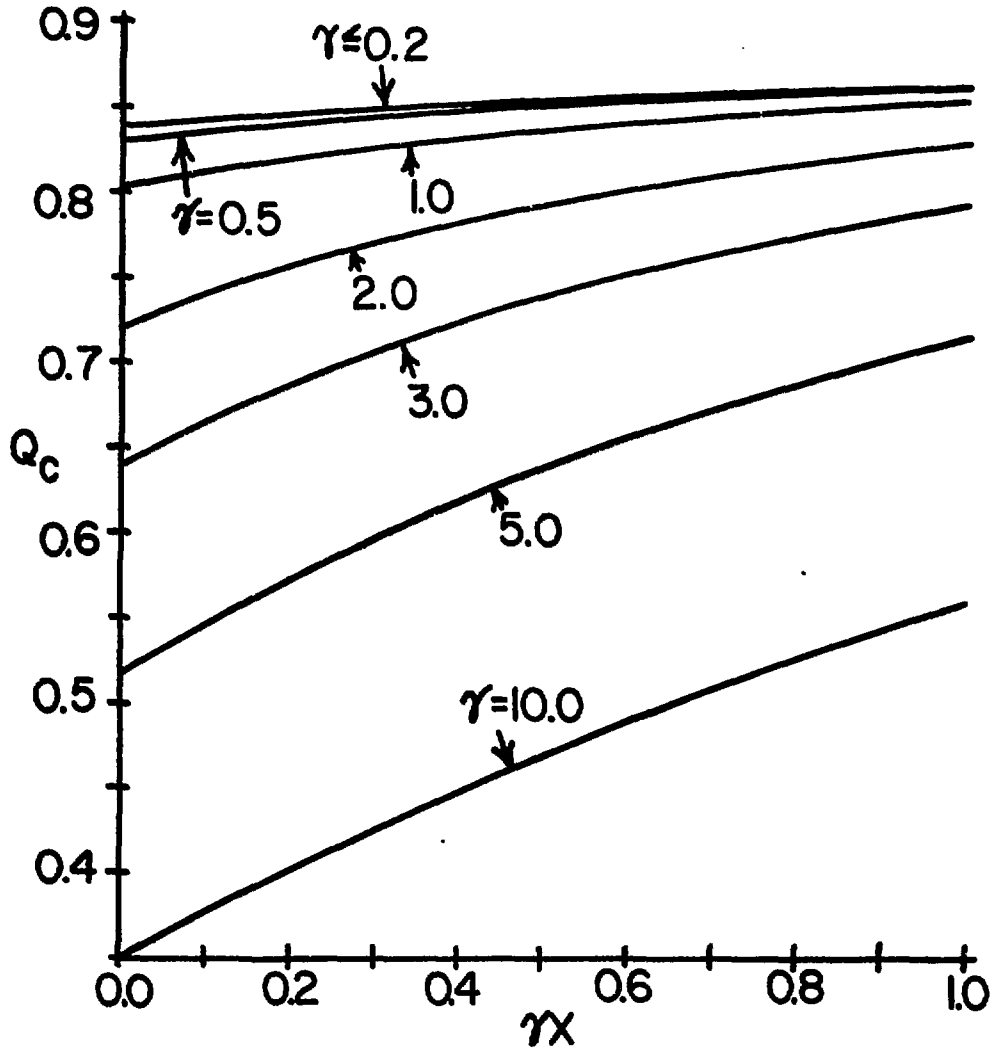

FIGURE 4e: Fraction of the total flow carried by the core, $Q_c(X)$, for $\alpha = a = 1$, $\beta = 2$ and various γ.

$z = \pm 1$ increases. The sheet jets in the side layers are associated with the current in the y direction in the side. Such currents require a voltage gradient so $\partial\phi_s(X,y,0)/\partial y$ is not zero. However, $\partial\phi_c/\partial y = 0$, so that there is a jump in the $O(1)$ ϕ across the side layer. In the z component of Ohm's law (5c), $\partial\phi/\partial z = O(M^{1/2})$ in the side layer; j_z cannot be $O(M^{1/2})$ since it is $O(c)$ at $z = \pm 1$, so u must be $O(M^{1/2})$ in order to produce a $\underset{\sim}{v} \times \underset{\sim}{B}$ to balance the large $\underset{\sim}{\nabla}\phi$. The equation (14b) gives

$$\int_0^\infty u_s(X,y,\zeta)\, d\zeta = B_y^{-1}\, \Delta\phi_s = B_y^{-1}[\phi_c(X,-1) - \phi_s(X,y,0)] \tag{25}$$

The boundary condition (16b) shows that $\Delta\phi_s = 0$ at $y = \pm a$. For $\alpha >> 1$, the first term in the equation (14e) dominates and $j_{zs}(X,y,0)$ is independent of y. The j_{yw} is linear in y in the side and

$$\Delta\phi_s = 3Q_s B_y (1 - y^2/a^2) \tag{26}$$

The sheet jet has a parabolic distribution of flow with y. In fact, the relationship (26) is relativley good for all values of α. The principal effect of reducing α is to permit some of the current to flow in the side layer rather than in the side, which reduces Q_s but does not change its parabolic distribution in y very much. As γ increases, the core flow becomes concentrated near $z = \pm 1$. This corresponds to an increase in the value of $\partial\phi_c/\partial z$ at $z = \pm 1$, which implies an increase in the electrical current in the z direction in the top and bottom at $z = \pm 1$. These currents must flow in the y direction in the side or side layer. Therefore $\Delta\phi_s$ and Q_s are proportional to $\partial\phi_c/\partial z$ at $z = \pm 1$ and increase as this voltage gradient increases.

The dependence of the results for the gradually varying field region on β are illustrated in Figure 5. Three-dimensional effects are primarily a function of the magnetic field gradient whose magnitude is reflected in the product $\gamma(\beta - 1)$, and there are some qualitative similarities of the results for different combinations of γ and β which have the same value of $\gamma(\beta - 1)$. However, these are only rough similarities. For $\beta = 2$ and $\gamma = 2$, there is 50%

reduction in field strength in a duct length $L_m = 0.5Lc^{-1/2}$, while for $\beta = 3$ and $\gamma = 1$, there is a 67% reduction in field strength in a duct length $L_m = Lc^{-1/2}$. Both cases give the same average magnetic field gradient, but the latter has a much larger average magnetic field strength than the former. Results depend on field gradient and field strength. The velocity profiles in Figure 5a are very similar to the corresponding ones in Figure 4a, so the velocity profile is primarily a function of field gradient. However, the pressure profiles in Figure 5b are quite different from the corresponding ones in Figure 4b for the larger values of β and γ. As β increases for a given γ, the variations of ξ becomes large enough to produce characteristic surfaces blocking the axial current near $z = 0$. This increases the effective electrical resistance to axial currents and decreases the axial electric currents in spite of increases in the axial voltage gradients. This is the same as the result of increasing γ for a given β. However, if γ is increased with fixed β, the decreasing electrical current is interacting with a constant magnetic field strength and produces a decreasing body force, a decreasing transverse pressure difference and a decreasing Δp_{3D}. On the other hand, if β is increased with fixed γ, then the decreasing electric current is interacting with an increasing magnetic field strength and produces an increasing body force, increasing transverse pressure difference, and increasing Δp_{3D}. The pressure differences depend on the magnetic field strength as well as its gradient.

The axial pressure variations for three values of β are shown in Figure 5c. The results for $\beta = 2$ are the same as those for γ^{-1} in Figure 4d. The curves for $\beta = 1.5$ are similar to those in Figure 4d for $\gamma = 0.5$, i.e., not far from locally fully developed flow. However, as β increases, the analogy fails. For $\beta = 3$ and $\gamma = 1$, the flow in the gradually varying field region is evolving toward a uniform core pressure and axial velocity as X increases much more rapidly than it does for $\beta = 2$ and $\gamma = 2$. Thus, there is only a small difference betweem p_c at $z = \pm 1$ and at $z = 0$ at $x = \gamma^{-1}$ for large β. This also explains the large variation of Q_c with X for large β in Figure 5d. With $\beta = 5$, the velocity profile at $X = 0$ is very non-uniform with a large value of $\partial\phi_c/\partial z$ at $z = \pm 1$. This drives a large current through the side and increases Q_s. As X increases B_y decreases by 80%, u_c evolves quickly toward a uniform value and $\partial\phi_c/\partial z$ at $z = \pm 1$ decreases appropriately.

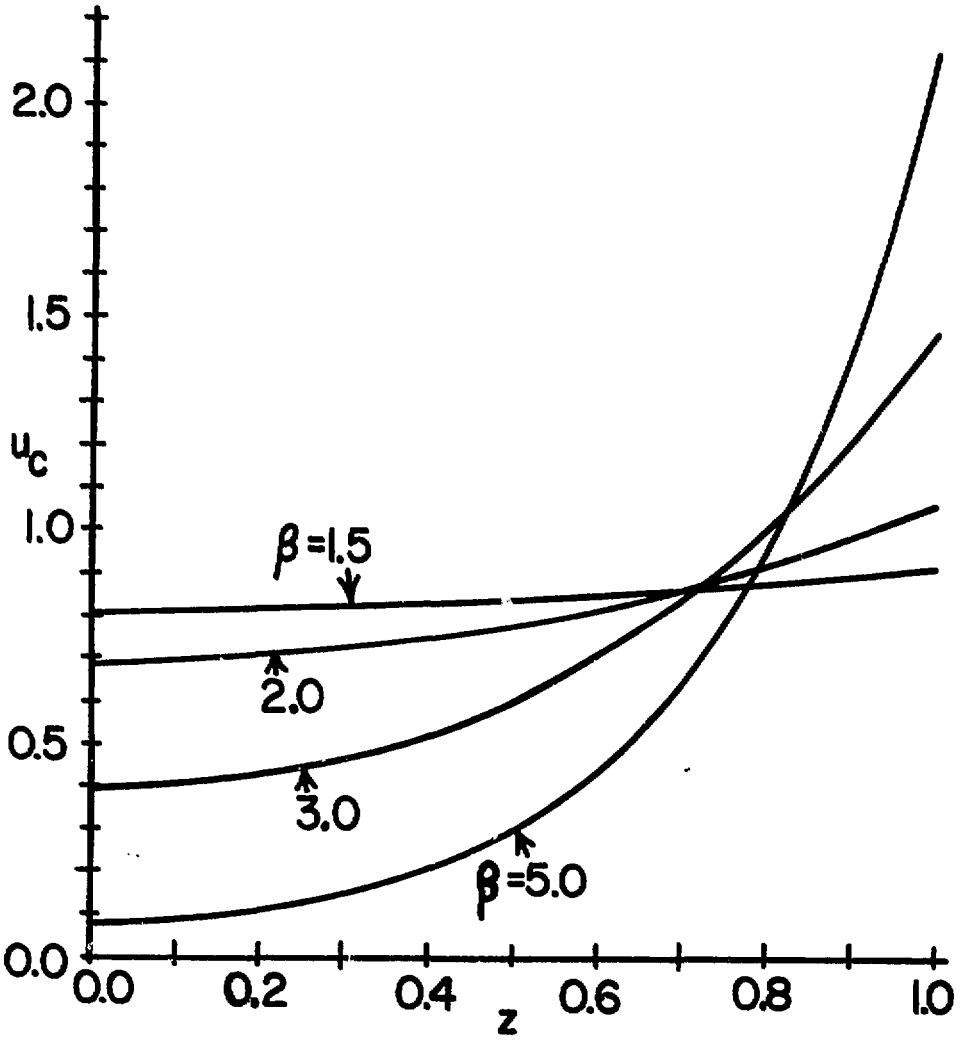

FIGURE 5a: u_c at X=0 for $\alpha = a = \gamma = 1$ and various β.

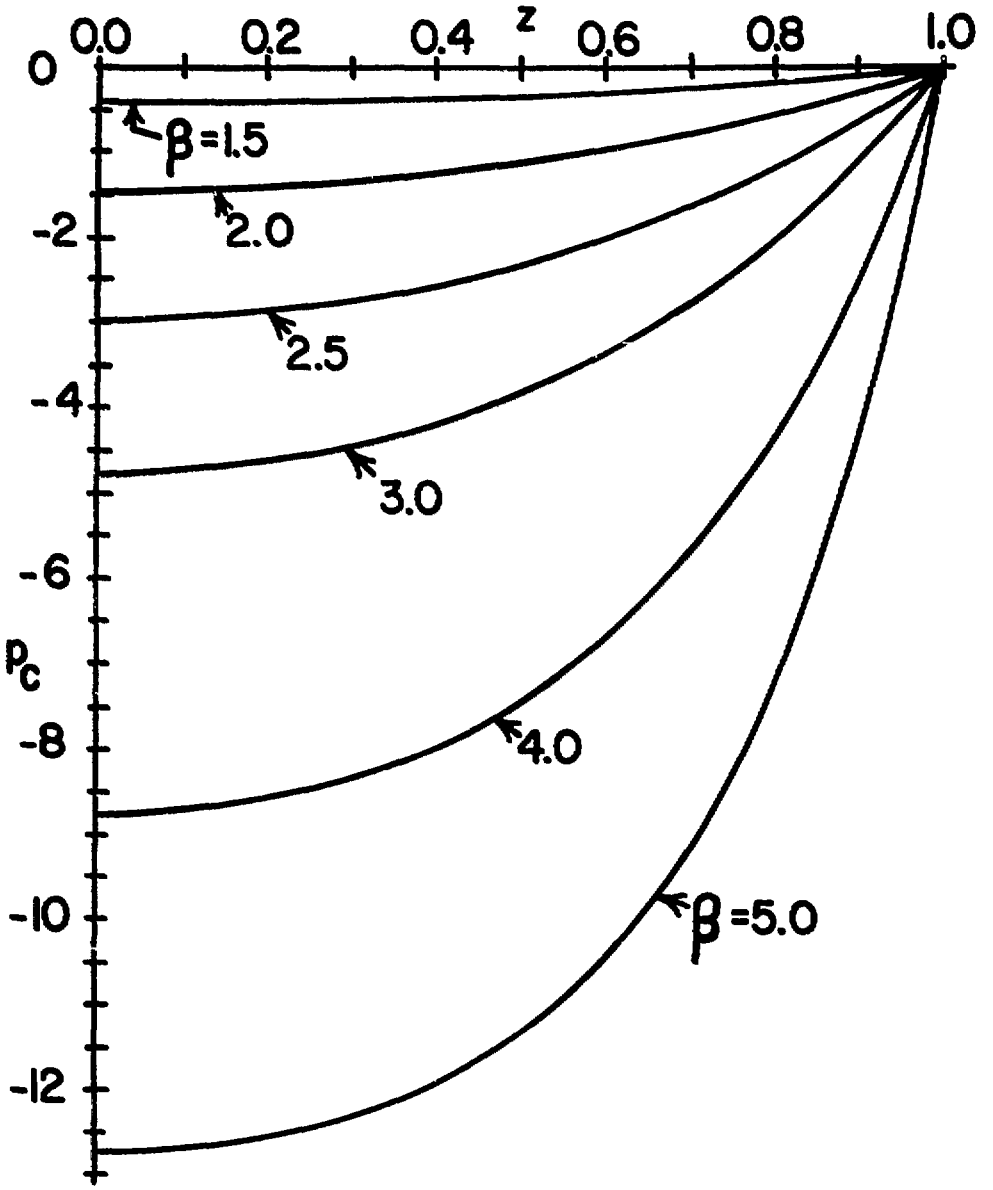

FIGURE 5b: p_c at X=0 for $\alpha = a = \gamma = 1$ and various β.

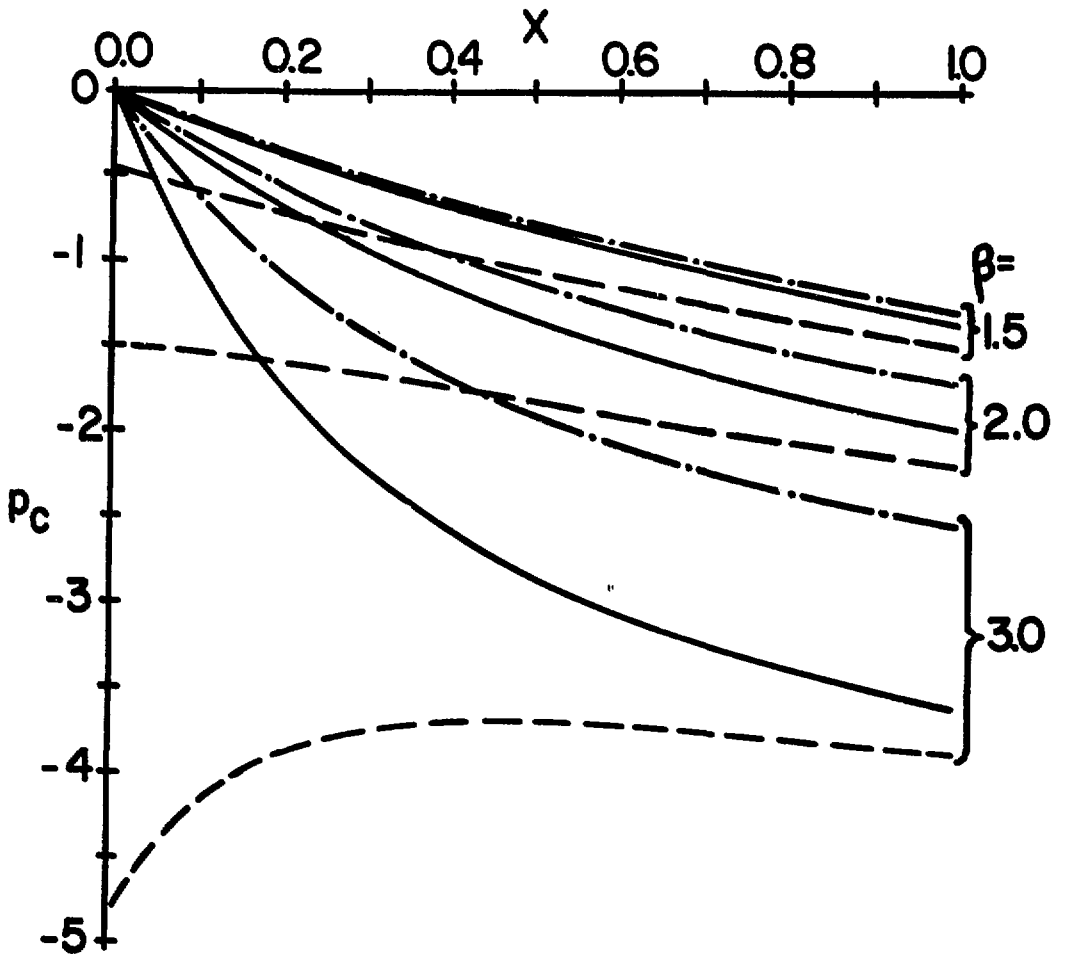

FIGURE 5c: p_c at z=1 (solid lines), p_c at z = 0 (dashed lines), and p_{fd} (dot-dash lines) for α = a = γ = 1 and various β.

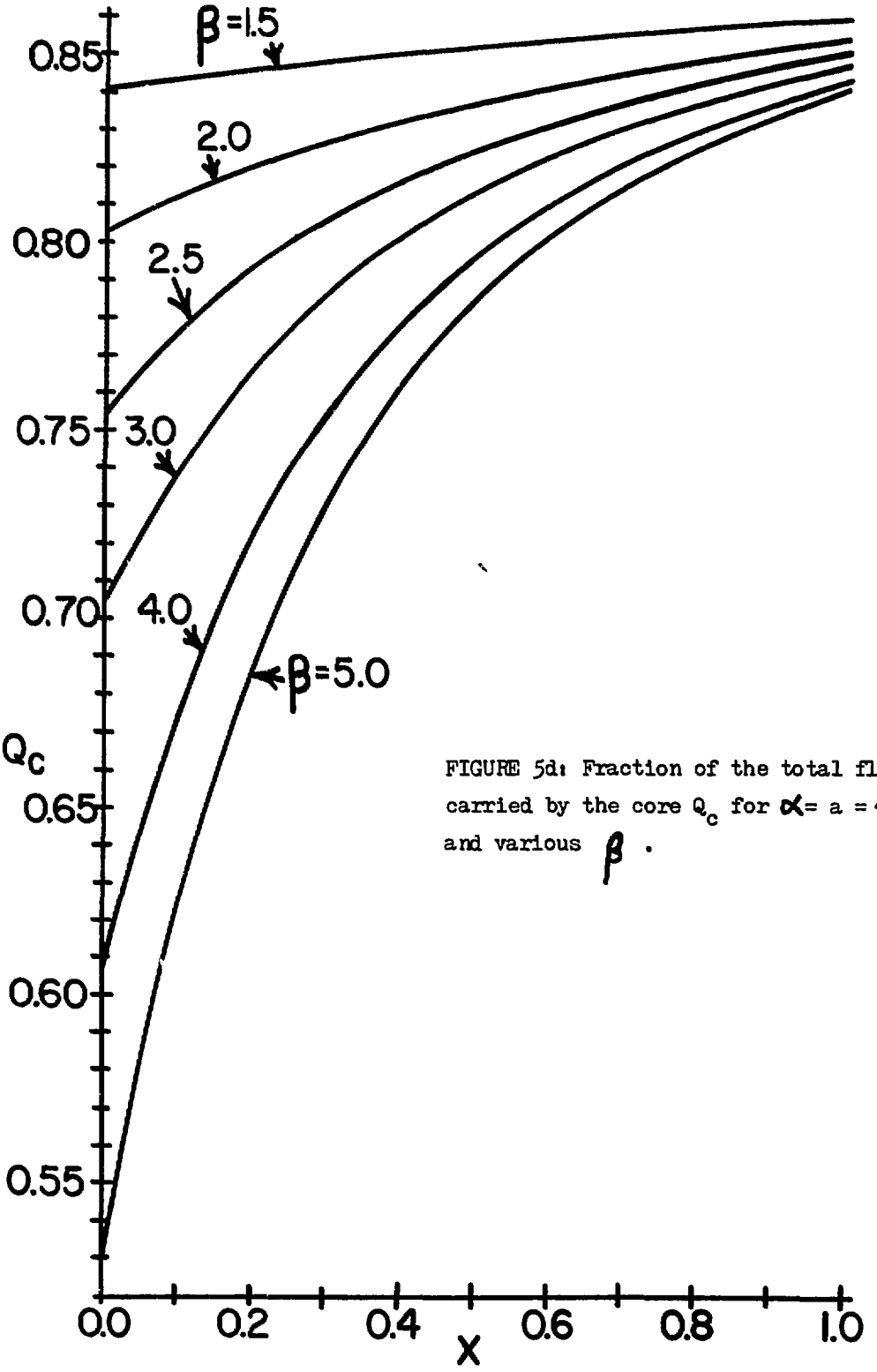

FIGURE 5d: Fraction of the total flow carried by the core Q_c for $\alpha = a = \gamma = 1$ and various β.

The dependence of the results for the gradually varying field region on α are illustrated in Figure 6. The variations of u_c at X = 0 in Figure 6a and of $Q_c(X)$ in Figure 6d are those expected. For larger values of α, more of the electric current in the y direction flows in the side, giving a relatively larger Q_s, so that Q_c and u_c are relatively smaller. Figures 6b and c indicate that all pressures, including that for locally fully developed flow, increases as α decreases. We have normalized the pressures with $c^{1/2}\sigma U_0 B_0{}^2 L$, so that we need to keep c constant to have a constant reference pressure. We should consider the wall thickness as constant and vary $\alpha = cM^{1/2}$ by varying M. The side and side layer are resistors in parallel and are part of the total electrical circuit. For $\alpha >> 1$, only the side carries current. As α decreases the side layer also starts to carry current so that the combined electrical resistance decreases. Reducing the resistance in one part of a circuit increases the current everywhere, so all pressure variations are increased. The analysis for $M^{-1/2} << c << 1$ is considerably easier than the present one for $c = \alpha M^{-1/2}$, but the former underestimates the pressure drops unless α is quite large--at least 10. For a duct with different wall thicknesses, the α which matters is that for the walls parallel to the magnetic field. At the other extreme, the results for $\alpha = 0.1$ still differ considerably from those for $M^{-1} << c << M^{-1/2}$.

The $O(c^{1/2})$ pressure at $z = \pm 1$ does not vary through either transition region, while the pressure at z = 0 changes through both transition regions to equal the value at $z = \pm 1$. These pressure changes are associated with the completion of the circuit for the axial electric currents in the gradually varying field region at X = 0 and γ^{-1}. Beyond each transition region is fully developed flow for $B_y = \beta$ or 1. Therefore, the difference between the overall pressure drop for the actual three-dimensional flow and that for the corresponding locally fully developed flow is simply $p_c(\gamma^{-1},\pm 1) - p_{fd}(\gamma^{-1})$. Expressed in dimensional terms, this pressure drop due to three-dimensional effects is

$$\Delta p_{3D} = Kc^{1/2}\, \sigma U_0 B_0^2 L \qquad (27)$$

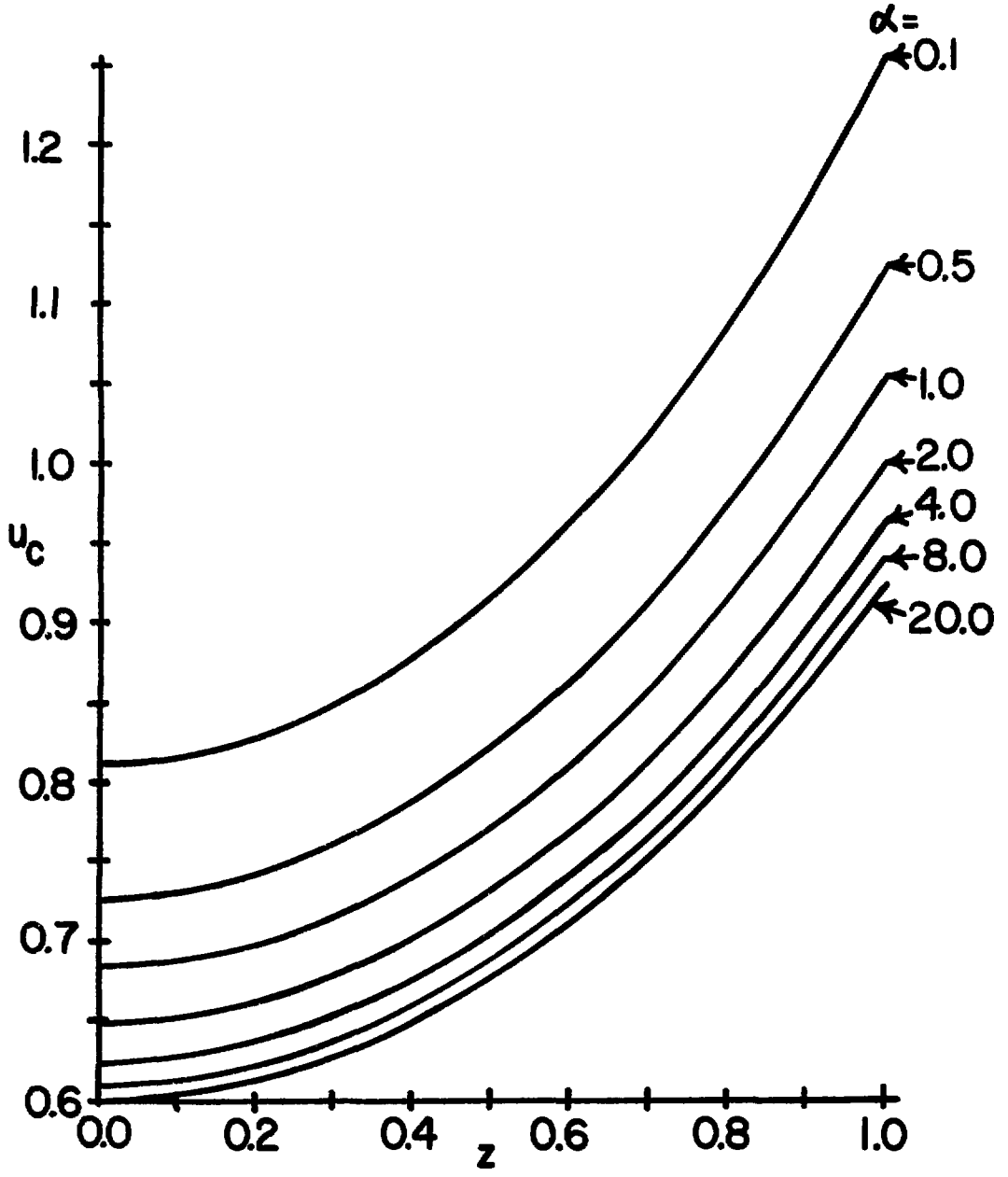

FIGURE 6a: u_c at X=0 for a = γ = 1, β = 2 and various α.

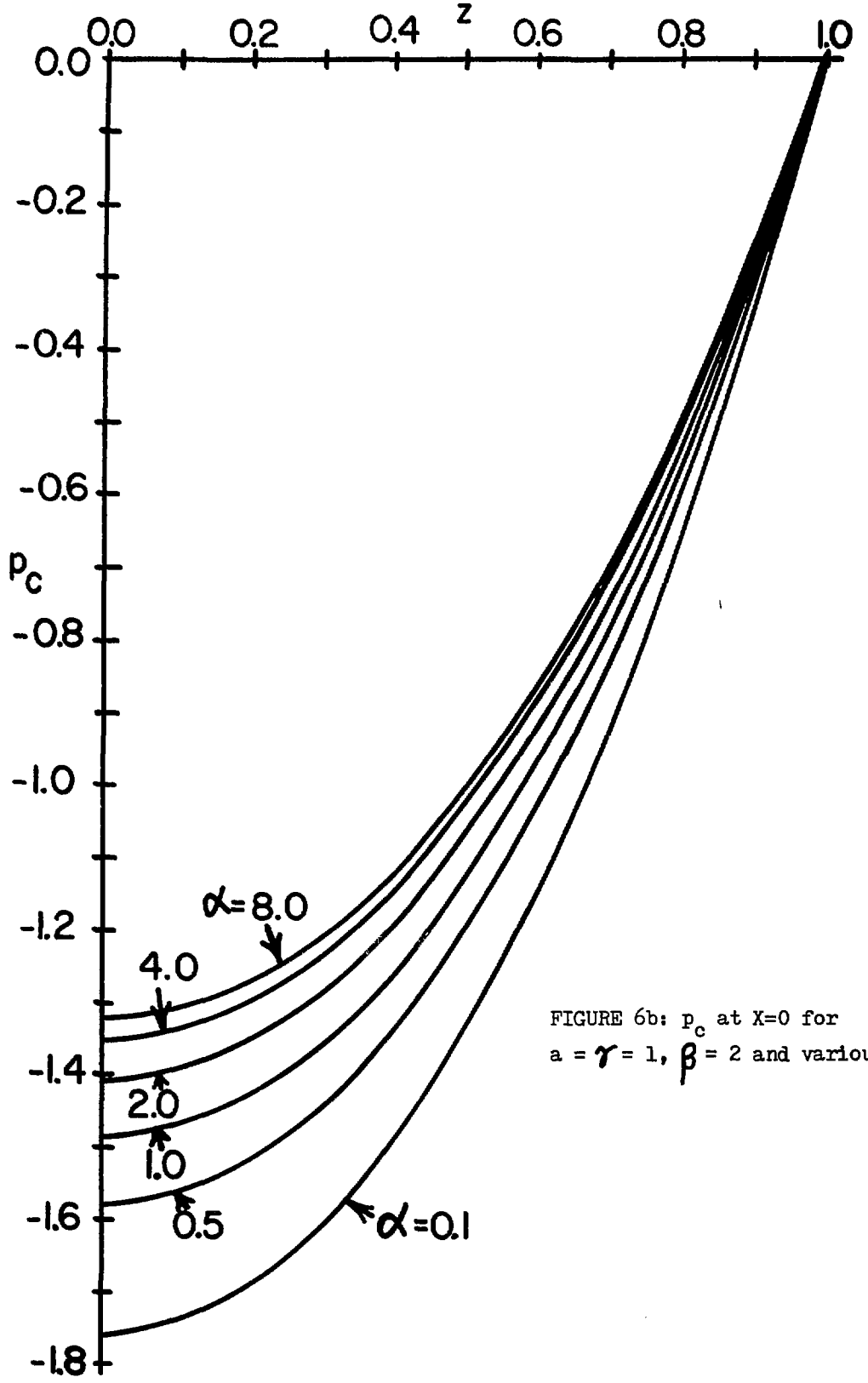

FIGURE 6b: p_c at X=0 for $a = \gamma = 1$, $\beta = 2$ and various α.

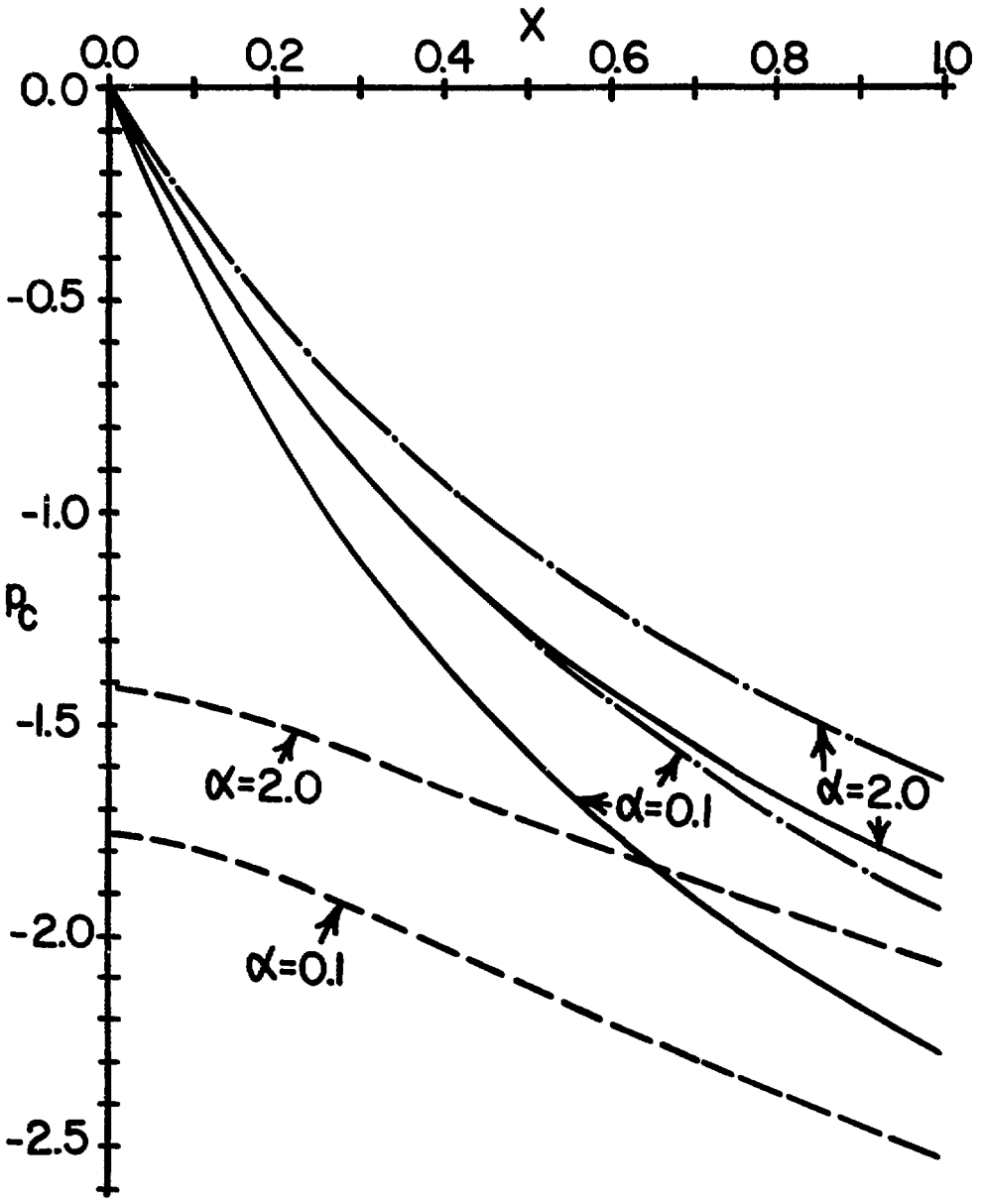

FIGURE 6c: p_c at z=1 (solid lines), p_c at z=0 (dashed lines)and p_{fd} (dot-dash lines) for a = γ = 1, β = 2 and various α.

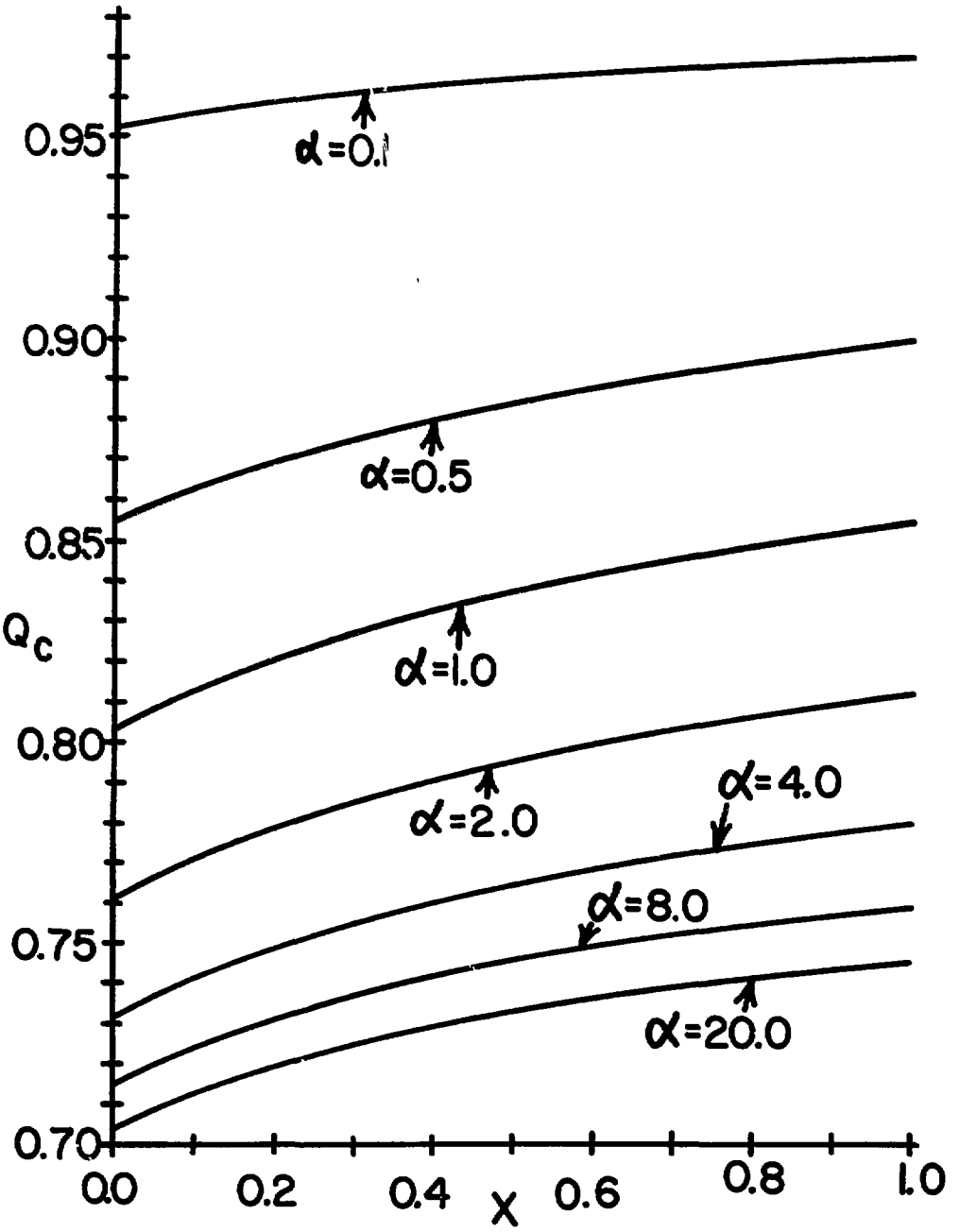

FIGURE 6d: Fraction of the total flow carried by the core Q_c for $a = \gamma = 1$, $\beta = 2$ and various α.

where the coefficient K depends on α, β, γ, and a, while B_0 is the strength of the weaker uniform magnetic field and L is half the distance between the walls parallel to the magnetic field. Since we can determine Δp_{3D} without solving for the transition regions, the present results are not restricted to the particular magnet geometry shown in Fiqure 1. The present results apply to any gradual variation of the transverse magnetic field. Here the upstream and downstream junctions add no additional $O(c^{1/2})$ pressure drops. In a fusion blanket, the magnetic field becomes uniform at one end of a radial duct because the duct turns to the axial direction. Such an elbow has no $O(c^{1/2})$ three-dimensional pressure drop [9]. If the "piping fixtures" at x = 0 and $x = \varepsilon^{-1}$ do have $O(c^{1/2})$ pressure drops, they can be summed with the present one as independent pressure losses. Figure 7 presents the values of K versus γ for various combinations of α and β. Again we see that Δp_{3D} (a) has a peak at a certain value of γ for each α and β, and decreases for larger γ, (b) always increases as β increases, and (c) always decreases as α increases.

4. UPSTREAM TRANSITION REGION FOR $L_m = L\gamma^{-1}c^{-1/2}$

In the upstream transition region the magnetic field is given by the equations (3). In the core for this region the solution of the equations (5) with the appropriate symmetry about y = 0 is

$$u_u = \beta^{-1} \frac{\partial \phi_u}{\partial z}, \quad w_u = -\beta^{-1} \frac{\partial \phi_u}{\partial x} \tag{28a,b}$$

$$v_u = \beta^{-2} y \left(\frac{\partial^2 p_u}{\partial x^2} + \frac{\partial^2 p_u}{\partial z^2} \right) - \gamma \beta^{-2} \frac{\partial \psi_u}{\partial x} \frac{\partial \phi_u}{\partial z} \tag{28c}$$

$$j_{xu} = \beta^{-1} \frac{\partial p_u}{\partial z}, \quad j_{zu} = -\beta^{-1} \frac{\partial p_u}{\partial x} \tag{28d,e}$$

$$j_{yu} = -\gamma \beta^{-2} \frac{\partial \psi_u}{\partial x} \frac{\partial p_u}{\partial z} \tag{28f}$$

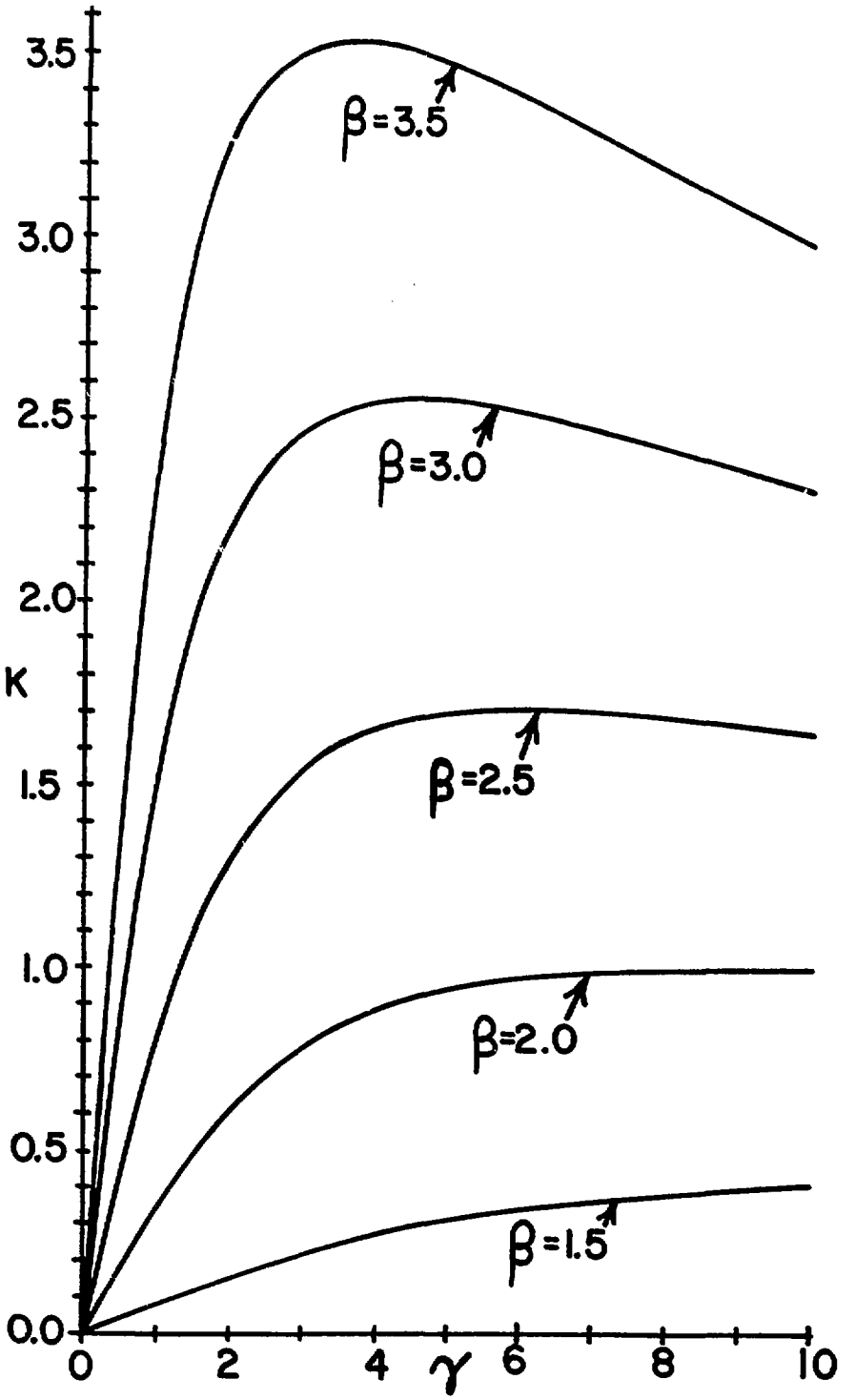

FIGURE 7a: Three-dimensional pressure drop coefficient for $\alpha = 0.1$.

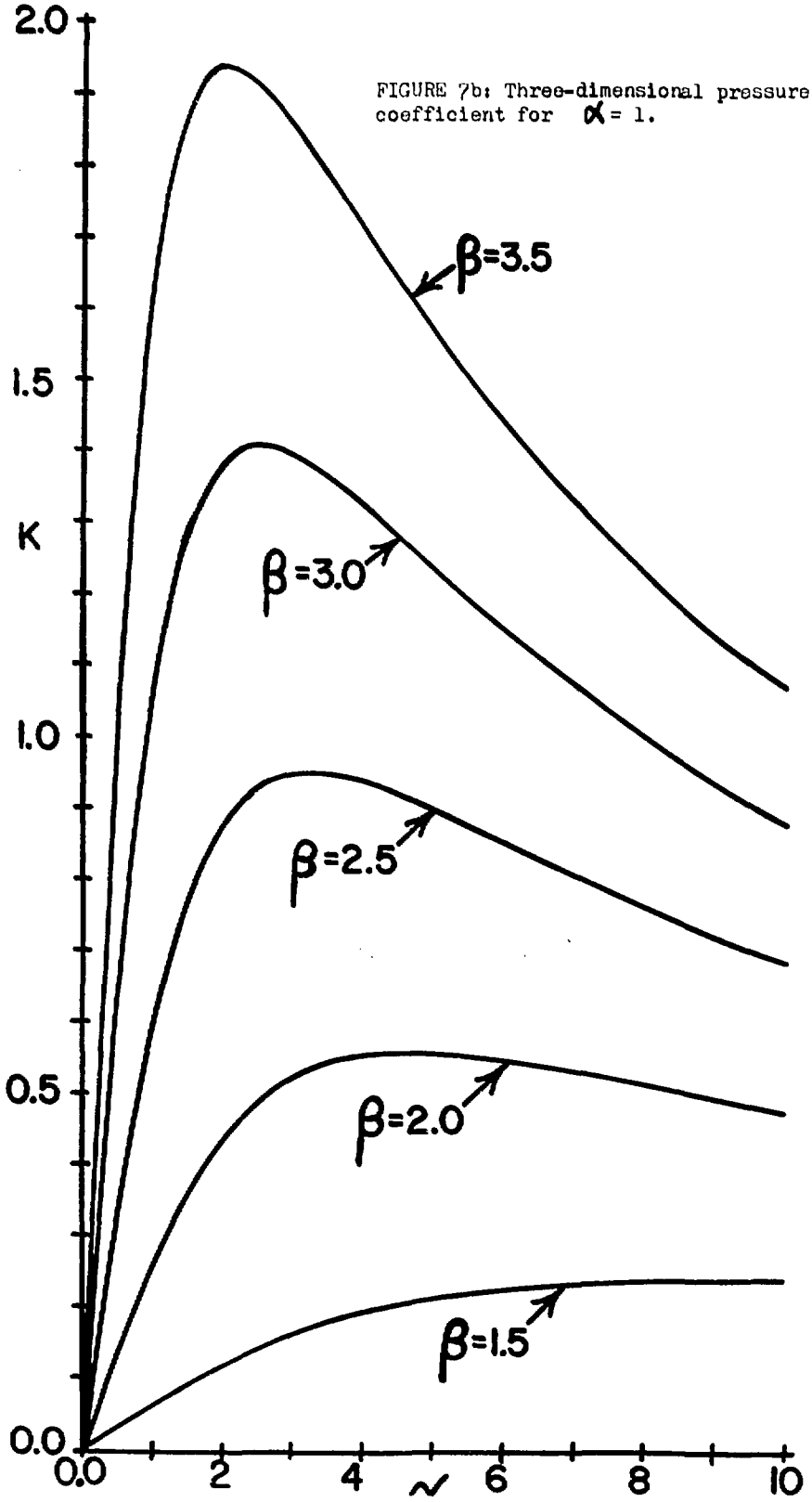

FIGURE 7b: Three-dimensional pressure drop coefficient for $\alpha = 1$.

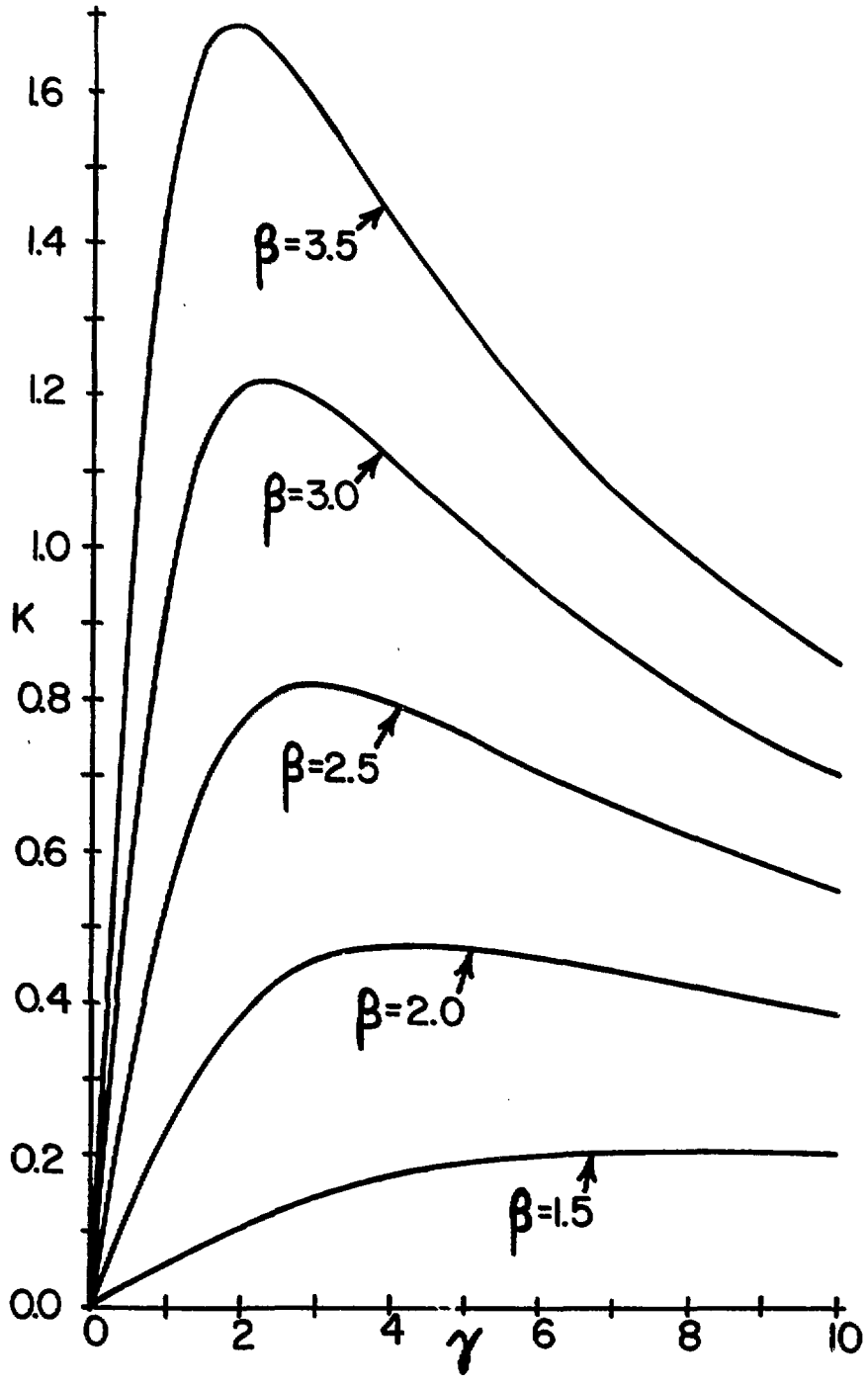

FIGURE 7c: Three-dimensional pressure drop coefficient for $\alpha = 2$.

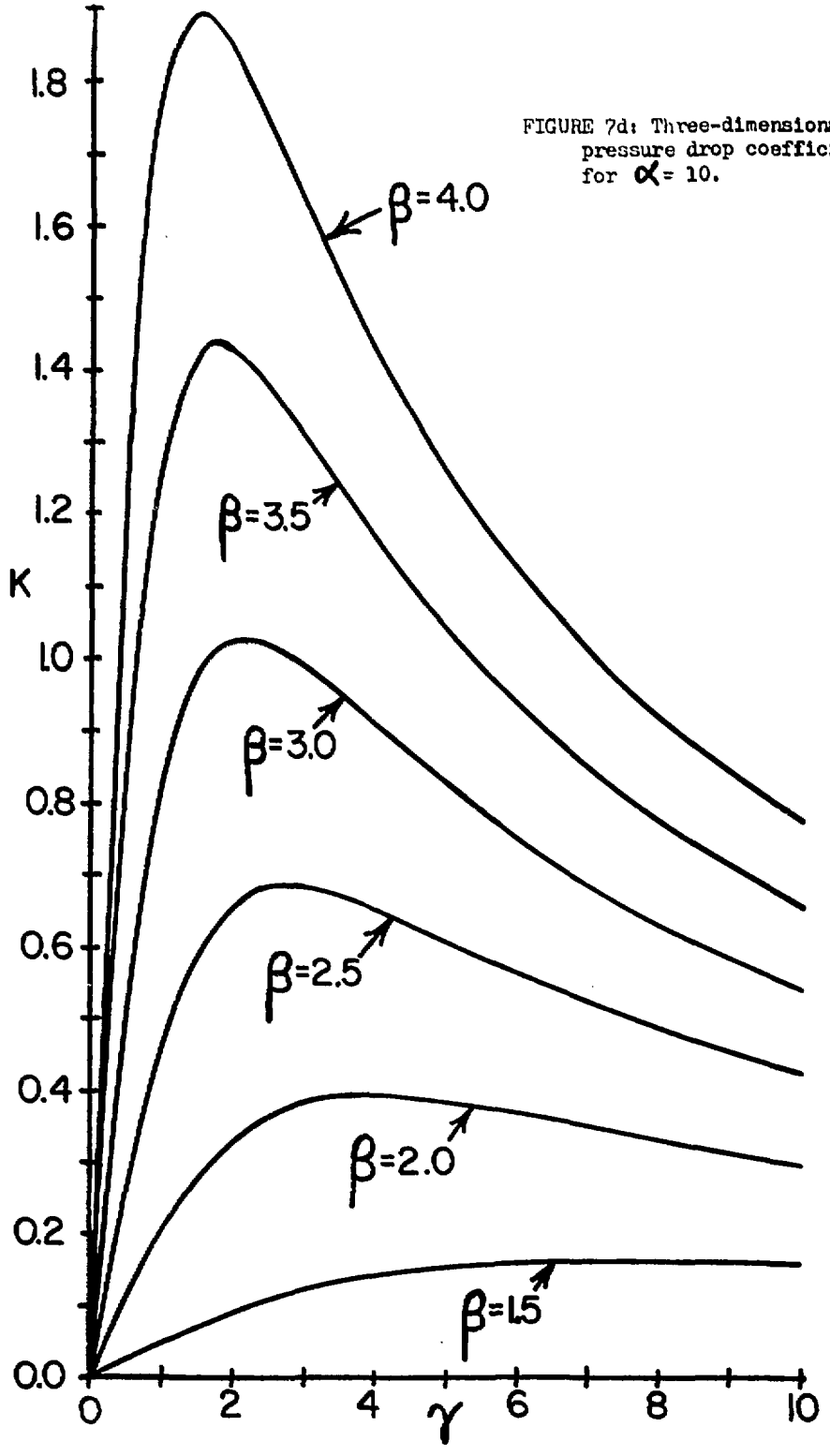

FIGURE 7d: Three-dimensional pressure drop coefficient for $\alpha = 10$.

Here u_u, w_u and ϕ_u are O(1); v_u, j_{xu}, j_{zu} and p_u are $O(c^{1/2})$; j_{yu} is O(c); $p_u(x,z)$ and $\phi_u(x,z)$ are unknown integration functions; $\psi_u(x,y)$ is given by equations (3c,d). The boundary conditions (7a, 11) give the equations governing p_u and ϕ_u,

$$\nabla^2 p_u = \gamma a^{-1} \frac{\partial \psi_u}{\partial x}(x,a) \frac{\partial \phi_u}{\partial z} \tag{29a}$$

$$\nabla^2 \phi_u = \gamma \beta^{-2} \frac{\partial \psi_u}{\partial x}(x,a) \frac{\partial p_u}{\partial z} \tag{29b}$$

for $-\infty < x < \infty$ and $-1 < z < 1$, where ∇^2 is the Laplacian with respect to x and z. The side layers cannot accept any $O(c^{1/2})$ electric current over an O(1) duct length since j_z is only O(c) in the side layers. Therefore, the equation (28e) and the condition $p = 0$ at $x = 0$ and $z = \pm 1$ give the boundary condition

$$p_u = 0, \quad \text{at } z = \pm 1 \tag{30}$$

We introduce the Fourier series solutions

$$p_u = \sum_{n=0}^{\infty} h_n(x) \cos(\kappa_n z) \tag{31a}$$

$$\phi_u = zG(x) + \sum_{n=0}^{\infty} g_n(x) \sin(\kappa_n z) \tag{31b}$$

where

$$\kappa_n = (n + \tfrac{1}{2})\pi, \quad G(x) = \frac{\partial \phi_u}{\partial z}(x,\pm 1) \tag{31c,d}$$

The boundary conditions (30) are satisfied and the equations (29) reduce to the ordinary differential equations

$$\frac{d^2h_n}{dx^2} = \kappa_n^2 h_n + \gamma a^{-1} \frac{\partial \psi_u}{\partial x}(x,a)\,[\kappa_n g_n + 2\kappa_n^{-1}(-1)^n G] \tag{32a}$$

$$\frac{d^2g_n}{dx^2} = \kappa_n^2 g_n - \gamma \beta^{-2} \kappa_n \frac{\partial \psi_u}{\partial x}(x,a)\, h_n - 2(-1)^n \kappa_n^{-2} \frac{d^2G}{dx^2} \tag{32b}$$

These equations are coupled to the side layer solution.

For the side layer at $z = -1$ in the upstream transition region, the equations (5) give

$$j_{zus} = -\beta^{-1} \frac{\partial p_{us}}{\partial x} + \beta^{-2} \frac{\partial^3 \phi_{us}}{\partial \zeta^3} \tag{33}$$

and the equations (14a-d,f-h) with (a) the subscript s replaced by us, (b) $B_y(X)$ replaced by the constant β, (c) X replaced by x, and (d) $\gamma = 0$. These equations apply for $-\infty < x < \infty$, $-a < y < a$, $0 < \zeta < \infty$. Here u_{us} and v_{us} are $O(M^{1/2})$; w_{us}, ϕ_{us}, j_{xus}, and j_{yus} are $O(1)$; j_{zus} and p_{us} are $O(M^{-1/2})$. Matching the adjacent core gives the boundary conditions

$$v_{us} \to 0,\ \phi_{us} \to \phi_u(x,-1),\ p_{us} \to \alpha P_u(x),\ \text{as } \zeta \to \infty \tag{34}$$

where $P_u(x)$ is the $O(c)$ perturbation pressure in the core evaluated at $z = -1$. Again the $O(1)$ ϕ_w is constant in the adjacent parts of the top and bottom [4], so that this fact and the boundary condition (11) give

$$v_{us} = 0,\ \phi_{us} = \phi_u(x,-1),\ \text{at } y = \pm a \tag{35}$$

The boundary conditions (7b, 9b) become

$$v_{us} = 0, \quad \frac{\partial \phi_{us}}{\partial \zeta} = 0, \quad \frac{\partial p_{us}}{\partial \zeta} = -\beta \frac{\partial \phi_{us}}{\partial x}, \tag{36a-c}$$

$$\alpha\beta^2 \left(\frac{\partial^2 \phi_{us}}{\partial x^2} + \frac{\partial^2 \phi_{us}}{\partial y^2} \right) = \frac{\partial^3 \phi_{us}}{\partial \zeta^3} - \beta \frac{\partial p_{us}}{\partial x}, \quad \text{at } \zeta = 0 \tag{36d}$$

When the total flow condition (10) is applied to a cross section of the upstream transition region, it gives the condition (18) with $\phi_s(X,y,0)$ replaced by $\phi_s(x,y,0)$ and with $CB_y(X)$ replaced by $-2a\beta$. The extension of the conservation of current condition (8a) parallels that leading to the equation (20) and gives

$$\frac{dP_u}{dx} = -\beta a^{-1} G(x) \tag{37}$$

The solutions of the modified equations (14f-h) with the boundary conditions (34, 35, 36a,b) are

$$v_{us} = \sum_{m=1}^{\infty} b_m(x) \sin(m\pi y/a) \exp(-\tau_m \zeta) \sin(\tau_m \zeta) \tag{38a}$$

$$p_{us} = \alpha P_u(x) + \beta \sum_{m=1}^{\infty} b_m(x) \cos(m\pi y/a) \exp(-\tau_m \zeta) \cos(\tau_m \zeta) \tag{38b}$$

$$\phi_{us} = \phi_u(x,-1) + \sum_{n=0}^{\infty} e_n(x) \cos[(2n+1)\pi y/2a] \exp(-\lambda_n \zeta) \times [\cos(\lambda_n \zeta) + \sin(\lambda_n \zeta)] \tag{38c}$$

where $\tau_m = (\beta m\pi/2a)^{1/2}$ and λ_n is given by the equation (21c) with B_y replaced by β so that each λ_n is now a constant instead of a function of X. The boundary condition (36c) determines the coefficients b_m in terms of e_n,

$$b_m = \tau_m^{-1} \sum_{n=0}^{\infty} \frac{de_n}{dx} R_{nm} \tag{39}$$

where

$$R_{nm} = (-1)^{(n+m)} \pi^{-1} \left[(n + m + \tfrac{1}{2})^{-1} + (n - m + \tfrac{1}{2})^{-1}\right]$$

The present version of the total flow condition (18) and the equation (38c) give

$$\phi_u(x,-1) = -\beta - \sum_{n=0}^{\infty} (-1)^n \kappa_n^{-1} e_n(x) \tag{40}$$

This must equal the core solution (31b) evaluated at $z = -1$, so that

$$G(x) = \beta + \sum_{n=0}^{\infty} (-1)^n \left[\kappa_n^{-1} e_n(x) - g_n(x)\right] \tag{41}$$

When we introduce the solutions (37, 38b,c, 39, 40) into the remaining boundary condition (36d), we obtain an ordinary differential equation for $e_n(x)$,

$$\frac{d^2 e_n}{dx^2} = \kappa_n^2 a^{-2} (1 + \alpha^{-1}\lambda_n^{-1}) e_n + 2\kappa_n^{-1} a^{-1} (-1)^n G \tag{42}$$

$$+ \sum_{k=0}^{\infty} \frac{d^2 e_k}{dx^2} \left[2(-1)^{(n+k)} \kappa_n^{-1} \kappa_k^{-1} - \alpha^{-1} \sum_{m=1}^{\infty} \tau_m^{-1} R_{nm} R_{km}\right]$$

The coupled equations (32, 41, 42) govern $e_n(x)$, $g_n(x)$, $h_n(x)$ and $G(x)$. Once these equations have been solved, the equations (28, 31) give all the core variables, while the modified equations (14a-d) and the equations (33, 38-40) give all the side layer variables. The equation (37) gives the variation of the O(c) pressure along the sides in the upstream transition region, but we have already neglected a comparable pressure drop in the gradually varying field region. The solutions of the equations (32, 41, 42) automatically match the fully developed flow solution for $B_y = \beta$ as $x \to -\infty$ and the solution in the gradually varying field region evaluated at $X = 0$ as $x \to -\infty$. Direct numerical integration of the coupled equations (32, 41, 42) is difficult because round-off errors grow exponentially with integration in either direction. Instead (a) we use a central difference for the second derivatives with $\Delta x = 0.2$ for $|x| < x_0$, (b) we assume that the second derivatives are zero at $x = \pm x_0$, (c) we truncate all infinite series with $n = n_0$ and $m = n_0 + 1$, and (d) we relax the solutions until the equations (32, 41, 42) are satisfied everywhere. Solutions with various x_0 and n_0 indicate that the results are the same for any $x_0 \geq 3$ and for any $n_0 \geq 9$. The series (31, 38) converge very rapidly so that only 10 terms in each give excellent results.

The value of the variable coefficient $\partial\psi_u/\partial x$ at $y = a$ depends on d. If the upstream pole faces touch the outside of the duct [$d = \beta(a + t/L)$] the magnet provides the most abrupt possible transition between the uniform and gradually varying magnetic fields. As the pole faces are moved away from the top and botto of the duct, the transition becomes more gradual. The results in Figure 8 are for the values $a = 1$, $d = 3$, $\alpha \gg 1$, $\beta = 2$, and $\gamma = 1$; results for other parameter values are similar. The transition from the uniform velocity and pressure for fully developed flow to the non-uniform ones for the flow in the gradually varying field region at $X = 0$ is illustrated in Figures 8a,b. This transition is associated with the completion of the circuit for the axial electric currents at $X = 0$. Axial variations are plotted in Figure 8c. As the flow becomes more concentrated near $z = \pm 1$, the values of $\partial\phi_u/\partial z$ at $z = \pm 1$ increase which drives more electric current into the corners at $y = \pm a$, $z = \pm 1$ and through the sides. Q_s increases proportionately and this reduces Q_c.

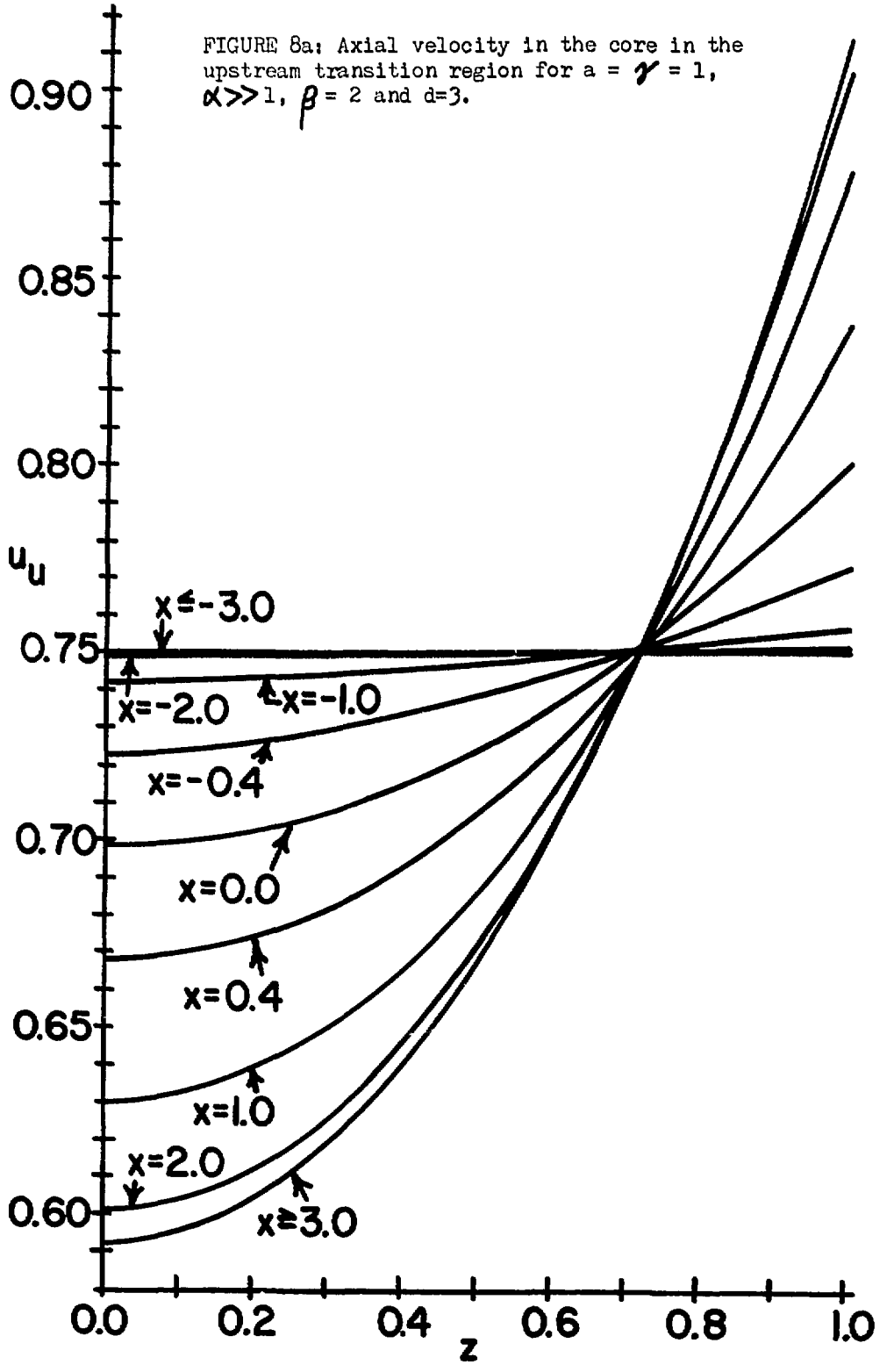

FIGURE 8a: Axial velocity in the core in the upstream transition region for a = γ = 1, $\alpha >> 1$, β = 2 and d=3.

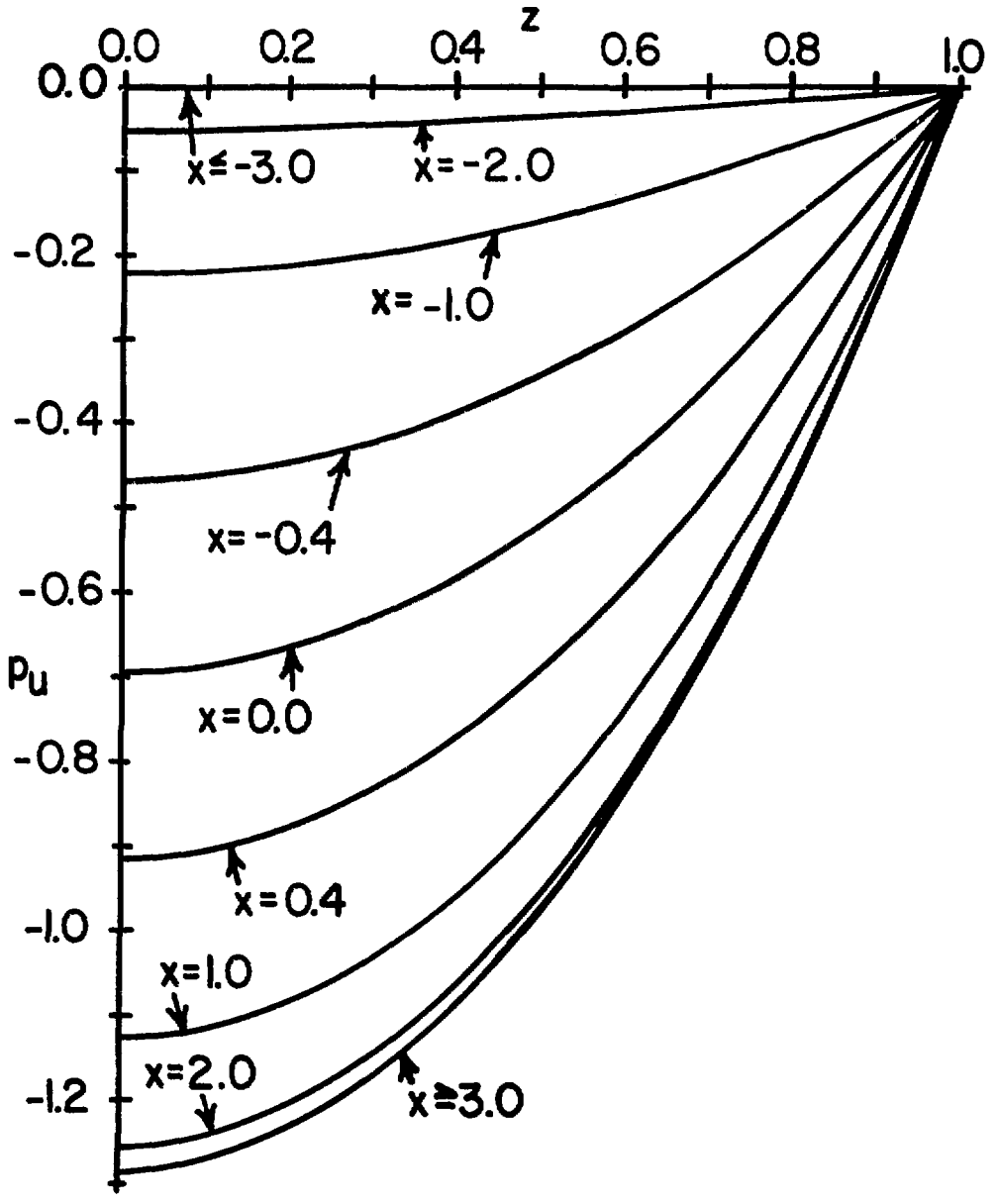

FIGURE 8b: Pressure in the core in the upstream transition region for a = γ = 1, $\alpha \gg 1$, β = 2 and d = 3.

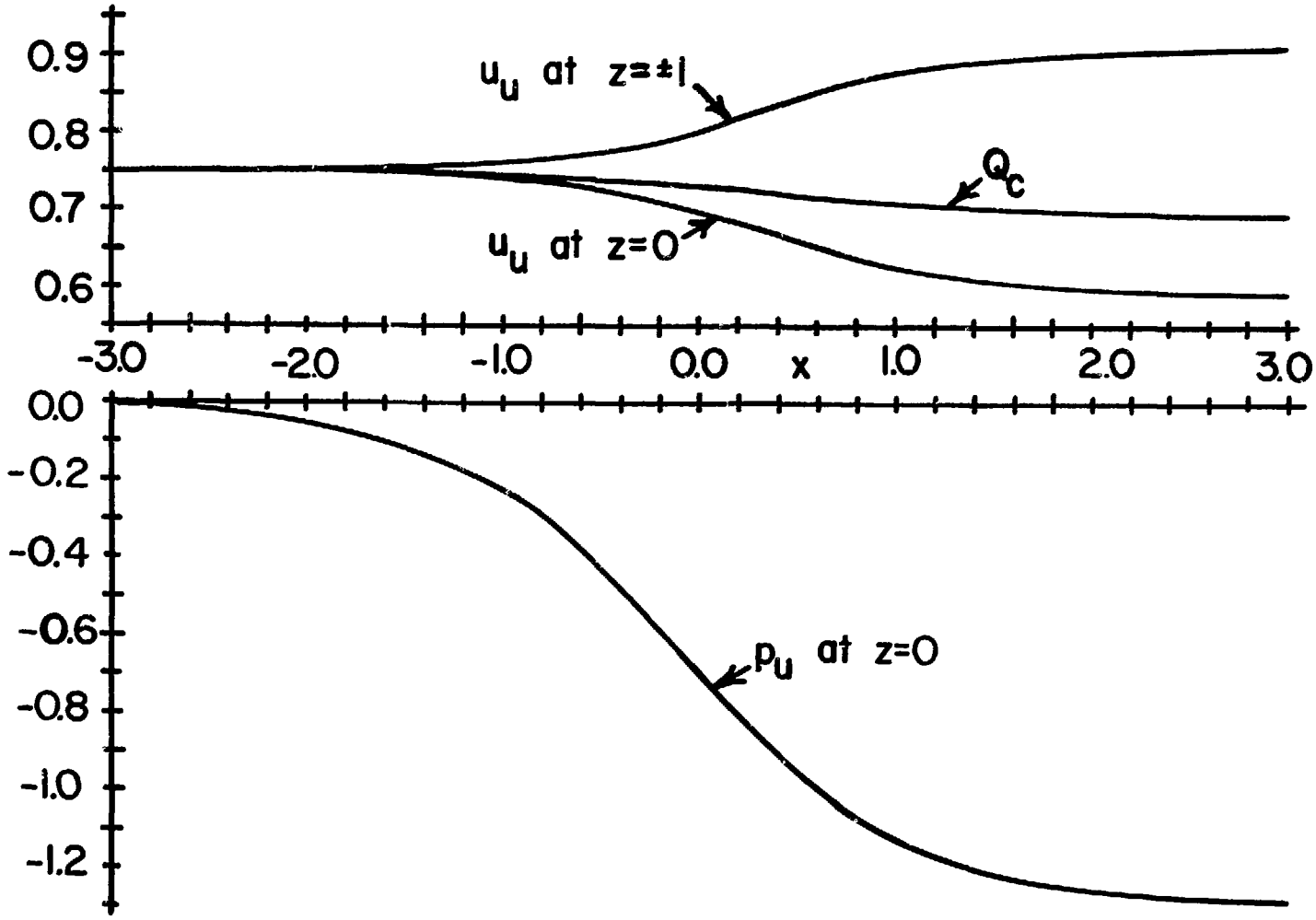

FIGURE 8c: Axial velocities, fraction of the flow in the core, and pressure at the centerline in the upstream transition region core for a= γ = 1, $\alpha \gg 1$, β = 2, and d = 3.

The analysis and results for the downstream transition region are very similar to the present ones for the upstream transition region. The transitions between the solution for the gradually varying field region at $X = \gamma^{-1}$ and the fully developed flow for $B_y = 1$ are much less dramatic than the present ones because u_c and p_c are much more uniform at $X = \gamma^{-1}$ than at $X = 0$. The magnetic field transition is also more gradual because the pole faces are further away from the duct. A composite solution which is valid for all x can be constructed by adding the solutions for the two transition regions and for the gradually varying field region with $X = xc^{1/2}$, and by subtracting the solutions for the gradually varying field region at $X = 0$ and at $X = \gamma^{-1}$. In order to get the correct pressure gradients far upstream and downstream, we should add

$$-c(1 + c)^{-1}\,\beta^2 x, \qquad -c(1 + 1)^{-1}(x - \varepsilon^{-1})$$

to the pressure for $x < 0$ and for $x > \varepsilon^{-1}$, respectively.

5. SOLUTIONS FOR $L \ll L_m \ll Lc^{-1/2}$

The solutions in sections 3 and 4 assume that the magnetic field gradient is $O(c^{1/2})$. Here we assume that this gradient is small, but much larger than $c^{1/2}$, i.e,. $c^{1/2} \ll \varepsilon = L/L_m \ll 1$. For the gradually varying field region in $0 < x < \varepsilon^{-1}$, we compress the axial coordinate by substituting $x = X\varepsilon^{-1}$. The magnetic field in each region is given by the equations (2-4) with γ and $c^{1/2}$ replaced by 1 and ε respectively. The Figure 2 is modified by the addition of outer side layers (o) with $O(c^{1/2}\varepsilon^{-1})$ thickness adjacent to the sides at $z = \pm 1$, while the side layers (s) with $O(M^{-1/2})$ thickness are now the inner side layers.

In the gradually varying field region for $0 < X < 1$, the axial velocities are $O(M^{1/2})$, $O(1)$ and $O(c)$ in the inner side layer, outer side layer and core, respectively. Therefore, the entire $O(1)$ flow required by the condition (10) is carried by the high velocity sheet jets in the inner side layers, while the total axial flows in the outer side layers and core are small, namely $O(c^{1/2}\varepsilon^{-1})$ and $O(c)$, respectively. The axial electric current densities j_x are $O(\varepsilon)$, $O(c^{1/2})$ and $O(\varepsilon c)$ in the inner side layer, outer side layer and core, respectively. Therefore, there is an $O(c\varepsilon^{-1})$ total axial electric

current in the $\pm x$ direction in the outer side layers at $z = \pm 1$, while the total axial currents in the inner side layers and core are much smaller, namely $O(\varepsilon M^{-1/2})$ and $O(\varepsilon c)$ respectively. As $\gamma \to \infty$ for the solution presented in sections 3 and 4: (a) the axial velocity and current in the core become blocked by the emerging characteristic surfaces, (b) the axial flow becomes concentrated in the inner side layers and (c) the axial current becomes concentrated in the outer side layers with an $O(c^{1/2}\varepsilon^{-1}) = O(\gamma^{-1})$ thickness. The $O(c\varepsilon^{-1})$ axial currents in the outer side layers have their maximum values at $X = 0$. The upstream leg of the circuit is completed by $j_z > 0$ in the upstream transition region. The downstream leg is completed through three parallel resistors: (a) the side layers, sides, top and bottom, (b) the downstream transition region at $x = \varepsilon^{-1}$, and (c) the core in the gradually varying field region where the $O(c)$ transverse current must follow the characteristic surfaces from one side layer to the other. The pressure at $z = 0$ drops enormously through the upstream transition region and then rises through the gradually varying field and downstream transition regions. The $O(c\varepsilon^{-1})$ pressure throughout the inner side layer $P_i(X)$ is given by the equation (23) with the one inside square bracket replaced by zero and with $B_y = \beta[1 + (\beta - 1)X]^{-1}$ in the equations (21c, 23). The pressure for locally fully developed flow is also $O(c\varepsilon^{-1})$ since this is the pressure drop for an $O(\varepsilon^{-1})$ duct length and is given by the equation (23). Therefore, the only difference between $P_i(X)$ and $P_{fd}(X)$ is the smaller denominator for P_i in the modified equation (23). The pressure throughout the core is

$$P_c(X) = P_i(X) + (\beta - 1)^{-1} [1 - (\beta - 1)X] \frac{dP_i}{dX}(X)$$

which always increases as X increases. The only transverse pressure variation occurs in the outer side layers and is associated with the sheet of $O(c\varepsilon^{-1})$ axial electric current here. The pressure in the outer side layer at $z = -1$ is given by

$$P_c + (P_i - P_c) \exp [-a^{1/2} (\beta - 1) \beta^{-1} B_y \varepsilon c^{-1/2} (z + 1)]$$

This corresponds to the limit of the solutions (13a,c) as $\gamma \to \infty$. As before, we can integrate the equations for P_i and p_{fd} numerically from X = 0 to X = 1. The difference at X = 1 represents the pressure drop due to three-dimensional effects, in addition to the pressure drop for the locally fully developed flow. Here the dimensional pressure drop has the form

$$\Delta p_{3D} = K' c\varepsilon^{-1} \sigma U_0 B_0^2 L = K' c\sigma U_0 B_0^2 L_m$$

where this coefficient K' represents the limit of γK as $\gamma \to \infty$. All the curve in Figure 7 are approaching hyperbolas given by $K'\gamma^{-1}$ as $\gamma \to \infty$. The values of K' for $1.5 \leq \beta \leq 4.0$ and for α = 1, 2 and 10 are plotted in Figure 9. If we plot the curves $K'\gamma^{-1}$ with the corresponding graphs in Figure 7, we find that the latter are slowly converging to these hyperbolas but are still below the hyperbolas by 20-30% at γ = 10. For practical values of c, γ = 10 corresponds to a value of L_m which is comparable to L. The present solution for $L << L_m << L_c^{-1/2}$ illustrates the mathematical transition between the asymptotic analysis for $L_m = O(L)$ and $c << 1$ [5] and the asymptotic solution for $L_m = O(Lc^{-1/2})$ and $c << 1$. However, for practical values of c, the analyses for $L_m = O(L)$ and for $L << L_m << L_c^{-1/2}$ lead to an unrealistically severe picture of the flow: all the flow is confined to sheet jets in the inner side layers and all the axial current is confined to current sheets in the outer side layers. In reality, the flow and current are becoming concentrated near z = ±1 but are still distributed over a significant part of the cross section even for $L_m = O(L)$. This part is still much too large to be considered a boundary layer. If we use the predictions of the analysis in sections 3 and 4 for all cases, we will neglect the interaction of the two transition regions when $L_m = O(L)$, but we will be much closer to reality and to realistic estimates of the pressure drop than either the analyses for $L_m = O(L)$ or for $L << L_m << L_c^{-1/2}$. If we use the composite solution described at the end of the last section we will remove part of the error of neglecting the interaction of the two transition regions for $L_m = O(L)$.

For $L << L_m << L_c^{-1/2}$, the transition regions accomplish the transition between the fully developed flows and the flow in the gradually varying field region, just as they do for $L_m = Lc^{-1/2}\gamma^{-1}$. However, the mathematical

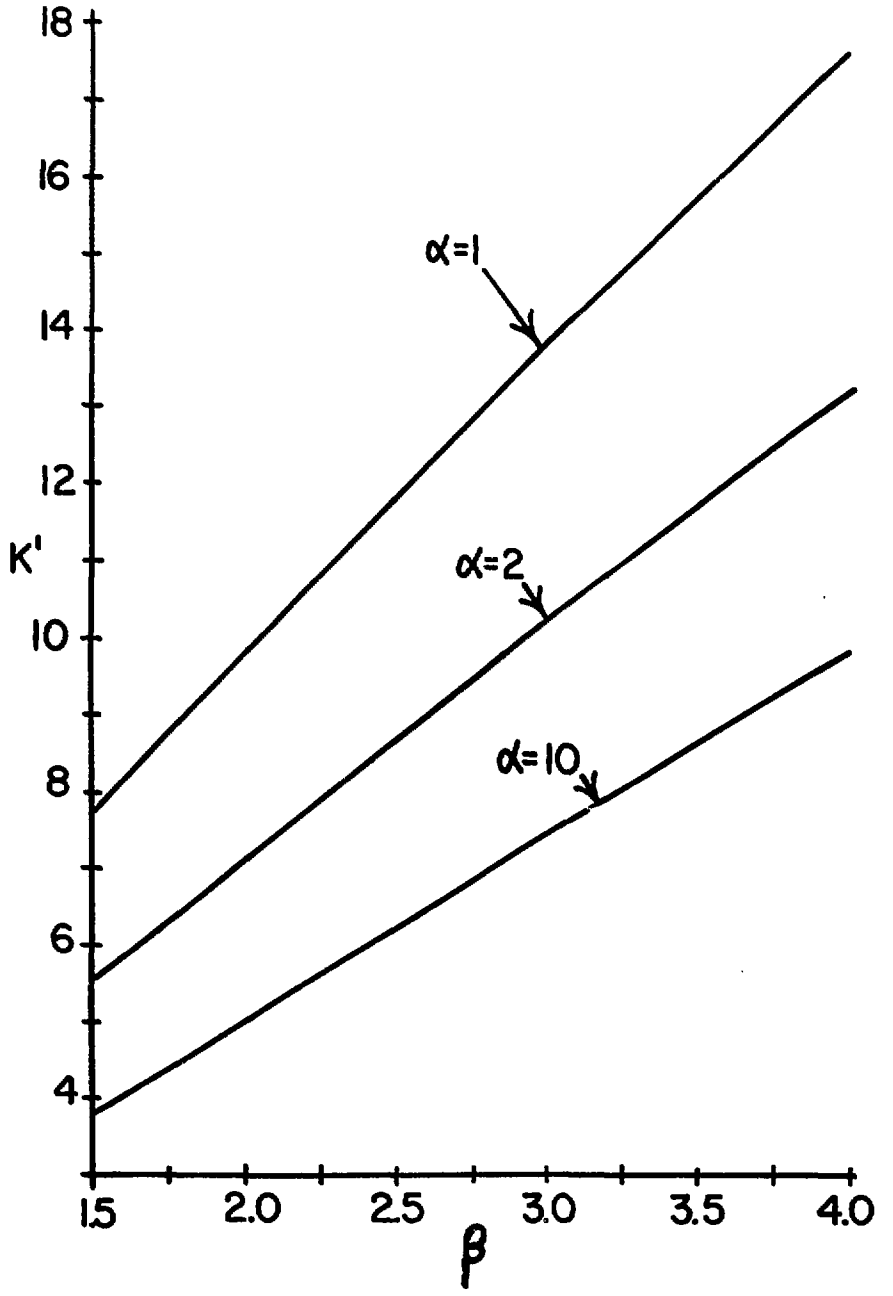

FIGURE 9: Three-dimensional pressure drop coefficient K' versus β for a = 1 and various α, where $L \ll L_m \ll L\, c^{-1/2}$

analysis is quite different. For $x = O(1)$, the magnetic field gradient is still large enough to create characteristic surfaces blocking the axial velocity and current in the core. We must go upstream from $x = 0$ until the magnitude of B_x, given by the equations (3b) with γ and $c^{1/2}$ replaced by 1 and ε, is $O(c^{1/2})$ rather than (ε). However, B_x decays exponentially so B_x is $O(c^{1/2})$ when $x = O[\ell n(c^{1/2}\varepsilon^{-1})]$. We compress the range $-\infty < x \leq 0$ into $0 < T \leq 1$ by substituting $x = (d/\beta\pi)\ \ell n\ (T)$. The exponentials in the equation (3d) are replaced by T^n. After the axial coordinate compression, there is a "boundary layer" with $O(\varepsilon^{-1}c^{1/2})$ thickness at $T = 0$, so we stretch the axial coordiante by substituting $T = \varepsilon^{-1}c^{1/2}\tau$. In the "boundary layer" only the first term in the infinite series (3d) remains as simply τ in the O(1) equations. This "boundary layer" is actually the upstream transition region which has been pushed upstream from $x = 0$ by the more severe magnetic field gradient. The core solution involves two integration functions $p_u(\tau,z)$ and $\phi_u(\tau,z)$ for $0 \leq \tau < \infty$ and $-1 \leq z \leq 1$, which are governed by coupled elliptic equations given by applying the boundary conditions (7a, 11). Fourier series in z again reduce the elliptic equations to ordinary differential equations in τ. These equations are similar to the equations (32) except that τ replaces $\partial\psi/\partial x$ and the equations are more complex because of the coordinate change. These equations are coupled to the side layer problem which is reduced to another ordinary differential equation. The equations are solved by relaxation on the range $0 \leq \tau \leq \tau_o$ for various τ_o. The results are similar to those presented in Figure 8. The $x = -3$ results correspond to $\tau = 0$, and as τ increases, the velocity and pressure becomes progressively more non-uniform. However, as $\tau \to \infty$, $p_u \to P_c(0)$ except near $z = \pm 1$ where a progressively steeper pressure gradient leads to the values $p_u = 0$ at $z = \pm 1$. This steep pressure gradient represents the emerging outer side layers. In addition, $u_u \to 0$ and all the flow migrates into the inner side layers as $\tau \to \infty$. Because of the large gradients, progressively more terms are needed in the Fourier series as τ_o is increased.

6. CONCLUSIONS

For the radial legs of a poloidal duct in a tokamak blanket, the toroidal magnetic field strength varies from 3 to 8 tesla over a duct length of 7.5 m, i.e., $B_o = 3$ tesla, $\beta = 2.67$ and $Lm = 7.5$ m [1]. If we take $c = 0.01$, $a = 1$,

and ℓ = 0.2 m [square ducts with 40 cm between the first and second walls], then γ = 0.267. If we also take M = 90,000, then α =3. For this case, the total pressure drop for the entire 7.5 m length of the duct is

$$81.4\ c\ \sigma\ U_0\ B_0^2\ L = 2.17\ c\ \sigma\ U_0\ B_0^2\ L_m$$

For the locally fully developed flow in this duct, the first coefficient above is replaced by 79.4, so that the actual pressure drop is only 2.5% more than that for locally fully developed flow. The maximum transverse variation of the axial velocity occurs at the inboard end of this duct where the magnetic field strength is 8 tesla. Here, the axial core velocity varies from $0.75U_0$ at the centerline to $0.827U_0$ near the first and second walls. Correspondingly, the fraction of the total flow in each of the side layers at this cross section is 0.112, while the value for locally fully developed flow here is 0.107. This flow deviates only slightly from locally fully developed.

On the other hand, where a feed pipe passes between the superconducting magnet coils, it sees a much larger magnetic field gradient, the flow is locally very different from fully developed flow. However, here the precise velocity profile is not particularly important because this is not a region where heat is deposited. If the three-dimensional pressure drops are large for these feed pipes, then perhaps one can use laminated pipe walls here because there is no danger of neutron damage to the electrically insulating ceramic materials between the structural metal and the thin metal liner in contact with the liquid metal.

ACKNOWLEDGMENTS

This research was supported by the U.S. Department of Energy through the Fusion Power Program at Argonne National Laboratory. Professor J. F. Donaldson provided computational assistance.

REFERENCES

[1] Smith, D. L, et al., "Blanket Comparison and Selection Study - Final Report," Argonne National Laboratory Report ANL-FPP-84-1, 1984.

[2] Holroyd, R. J. and Walker, J. S., "A theoretical study of the effects of wall conductivity, non-uniform magnetic fields and variable-area ducts on liquid-metal flows at high Hartmann number," (J. Fluid Mech., Vol. 84, 1978, pp. 471-495).

[3] Walker, J. S., "Liquid metal flow in a thin conducting pipe near the end of a region of uniform magnetic field," (J. Fluid Mech., 1986).

[4] Walker, J. S., "Magnetohydrodynamic flows in rectangular ducts with thin conducting walls. Part 1. Constant-area and variable-area ducts with strong uniform magnetic fields," (J. Mecan., Vol. 20, 1981, pp. 79-112).

[5] Walker, J. S., "Three-dimensional laminar MHD flows in rectangular ducts with thin conducting walls and strong transverse non-uniform magnetic fields," (Liquid-Metal Flows and Magnetohydrodynamics, ed. by H. Branover, P. Lykoudis and A. Yakhot, AIAA, 1983, pp. 3-19).

[6] Shercliff, J. A., "A Textbook of Magnetohydrodynamics", Pergamon Press, Oxford, 1965.

[7] Walker, J. S., "Liquid metal MHD flow in a duct whose cross section changes from a rectangle to a trapezoid with applications in fusion blanket designs," submitted for publication.

[8] Hoffman, M. A. and Carlson, G. A., "Calculation techniques for estimating the pressure losses for conducting fluid flows in magnetic fields," Lawrence Radiation Laboratory Report UCRL-51010, 1971.

[9] Walker, J. S., "Liquid metal flow through a thin conducting elbow in a plane perpendicular to a uniform magnetic field," submitted for publication.

Distribution for ANL/FPP/TM-207

Internal:

C. Baker
J. Bailey
M. Billone
J. Brooks
Y. Cha
D. Ehst
K. Evans
H. Geyer
Y. Gohar
P. Finn
A. Hassanein
Y. Liu
S. Majumdar
R. Mattas
B. Misra
M. Petrick
B. Picologlou
C. Reed
D. L. Smith
D. K. Sze
L. Turner
FPP Files (53)
ANL Contract File
ANL Libraries
ANL Patent Dept.
TIS Files (6)

External:

DOE-TIC, for distribution per UC-20 (107)
Manager, Chicago Operations Office, DOE
University of Chicago Special Committee for the Fusion Program:
S. Baron, Brookhaven National Laboratory
H. K. Forsen, Bechtel National, Inc., San Francisco
J. A. Maniscalco, TRW, Inc., Redondo Beach
G. H. Miley, U. Illinois, Urbana
P. J. Reardon, Brookhaven National Laboratory
P. H. Rutherford, Princeton University
D. Steiner, Rensselaer Polytechnic Institute
K. R. Symon, Synchrotron Radiation Center, Stoughton, WI
K. I. Thomassen, Lawrence Livermore National Laboratory
M. A. Abdou, University of California-Los Angeles
Ch. Alexion, Westinghouse Research and Development
R. G. Alsmiller, Oak Ridge National Laboratory
V. C. Baker, Oak Ridge National Laboratory
L. Barleon, KfK, Federal Republic of Germany
K. Barry, The Ralph Parsons Company
S. Berk, DOE
L. A. Berry, Oak Ridge National Laboratory
M. R. Bhat, Brookhaven National Laboratory
B. L. Bishop, Oak Ridge National Laboratory
J. A. Blair, Oak Ridge National Laboratory
A. L. Boch, Oak Ridge National Laboratory
K. H. Bockhoff, Commission of the European Communities
A. Bolon, University of Missouri-Columbia
L. Booth, Los Alamos National Laboratory
H. Branover, Ben Gurion University at the Negev, Israel
R. Brown, Los Alamos National Laboratory
R. Brown, School of Chemical Engineering, MIT
S. Burnett, GA Technologies, Inc.
D. Campbell, Oak Ridge National Laboratory
J. Cannon, Oak Ridge National Laboratory
G. Carlson, Lawrence Livermore National Laboratory
L. Carter, Hanford Engineering Development Laboratory
G. Casini, C.E.A. Ispra (VA), Italy
C. Clifford, Princeton Plasma Physics Laboratory
R. Conn, University of California-Los Angeles

J. Crocker, EG&G Idaho, Inc.
D. Dudziak, Los Alamos National Laboratory
P. Dunn, University of Notre Dame
M. J. Embrechts, Rensselaer Polytechnic Institute
C. Flanagan, Oak Ridge National Laboratory
K. Furuta, University of Tokyo, Japan
A. Gabriel, Oak Ridge National Laboratory
J. Garner, TRW, Inc., Redondo Beach
D. Graumann, GA Technologies, Inc.
H. Gruppelaar, Netherlands Energy Research Foundation
R. Hancox, Culham Laboratory, U.K.
G. Haste, Oak Ridge National Laboratory
M. Hoffman, University of California, Davis
R. Holroyd, Culham Laboratory, U.K.
R. Howerton, Lawrence Livermore National Laboratory
W. H. Hughes, Carnegie Melon University
J. Hunt, Cabridge University, U.K.
S. Iwasaki, Lawrence Livermore National Laboratory
D. Jassby, Princeton Plasma Physics Laboratory
R. J. Juzaitis, Los Alamos National Laboratory
S. Kailas, Indiana University
A. C. Klein, Oregon State University
H. Klein, Physikalisch-Technische Bundesanstalt
D. Kline, University of Texas
A. Knoblock, Max-Planck Institute fur Plasmaphysik, West Germany
R. A. Krakowski, Los Alamos National Laboratory
H. Kranse, Max-Planck Institute fur Plasmaphysik, West Germany
J. Kristiak, Slovak Academy of Sciences
G. Kulcinski, University of Wisconsin-Madison
R. A. Lillie, Oak Ridge National Laboratory
R. J. Livak, Los Alamos National Laboratory
B. G. Logan, Lawrence Livermore National Laboratory
G. Longo, Istituto di Fisica
C. Lund, San Diego State
P. S. Lykoudis, Purdue University
S. Malang, KfK, Federal Republic of Germany
J. Maniscalco, TRW
C. Marinucci, SIN, Villigen, Switzerland
C. Maynard, University of Wisconsin-Madison
H. McCurdy, Oak Ridge National Laboratory
R. Miller, Los Alamos National Laboratory
R. Moir, Lawrence Livermore National Laboratory
D. Montgomery, Massachusetts Institute of Technology
U. Muller, KfK, Federal Republic of Germany
K. Oishi, Shimizu Construction Co., Ltd.
Y. Oka, University of Tokyo, Japan
D. Paul, Electric Power Research Institute
S. Pearlstein, Brookhaven National Laboratory
E. Pierson, Purdue University, Calumet
J. Planquant, MOL, Belgium
J. Powell, Brookhaven National Laboratory
R. J. Puigh, Westinghouse Hanford Company
J. Ramos, Carnegie Melon University
J. Rathke, Grumman Aerospace Corporation

C. Rhilis, CEA
R. P. Rose, Westinghouse Electric Corporation
R. Roussin, Radiation Shielding Information Center, ORNL
E. Salpietro, NET - IPP
K. R. Schultz, GA Technologies, Inc.
H. Sebening, KfK, Federal Republic of Germany
Y. Seki, Japan Atomic Energy Research Institute
T. Shannon, Oak Ridge National Laboratory
Z. Shapiro, Westinghouse Electric Corporation
N. Sondergaard, David Taylor Naval Ship Research and Development Center
E. M. Sparrow, NSF
W. Stacey, Jr., Georgia Institute of Technology
M. Stauber, Grumman Aerospace Corporation
D. Steiner, Rensselaer Polytechnic Institute
J. D. Stout, Oak Ridge National Laboratory
K. Sumita, Osaka University, Japan
M. A. Sweeney, Sandia National Laboratories
A. Takahashi, Osaka University
D. Temperley, University of Ediuburgh, U.K.
K. I. Thomassen, Lawrence Livermore National Laboratory
W. L. Thompson, Los Alamos National Laboratory
A. Tsechanski, Ben Gurion University of the Negev
A. Tsinober, Tel Aviv University, Israel
J. Turner, DOE
J. Walker, University of Illinois
J. L. Walnier, MOL, Belgium
P. Walstrom, University of Wisconsin
D. Wattecamps, Commission of the European Communities
G. L. Woodruff, University of Washington-Seattle
V. Zoita, Central Institute of Physics, Bucharest
Librarian, Culham Laboratory, Oxford, England
Library, Centre de Recherches en Physique des Plasma, Lausanne, Switzerland
Library, FOM-Institue voor Plasma-Fysika, The Netherlands
Library Laboratorio Gas Ionizati, Frascatti, Italy
Thermonuclear Library, Japan Atomic Energy Research Institute, Tokyo, Japan